Since January 2020 Elsevier has created a COVID-19 resource centre with free information in English and Mandarin on the novel coronavirus COVID-19. The COVID-19 resource centre is hosted on Elsevier Connect, the company's public news and information website.

Computational Biology and Chemistry 99 (2022) 107692

Contents lists available at ScienceDirect

Computational Biology and Chemistry

journal homepage: www.elsevier.com/locate/cbac

Interaction of the new inhibitor paxlovid (PF-07321332) and ivermectin with the monomer of the main protease SARS-CoV-2: A volumetric study based on molecular dynamics, elastic networks, classical thermodynamics and SPT

Ysaias José Alvarado [a,*], Yosmari Olivarez [b], Carla Lossada [a], Joan Vera-Villalobos [c], José Luis Paz [d], Eddy Vera [b], Marcos Loroño [e], Alejandro Vivas [b], Fernando Javier Torres [f,g], Laura N. Jeffreys [h], María Laura Hurtado-León [i], Lenin González-Paz [i,j,**]

[a] Instituto Venezolano de Investigaciones Científicas (IVIC), Centro de Investigación y Tecnología de Materiales (CITeMA), Laboratorio de Caracterización Molecular y Biomolecular, 4001 Maracaibo, Bolivarian Republic of Venezuela
[b] Universidad del Zulia (LUZ). Facultad Experimental de Ciencias (FEC), Departamento de Quimica, Laboratorio de Electronica Molecular, 4001 Maracaibo, Bolivarian Republic of Venezuela
[c] Facultad de Ciencias Naturales y Matemáticas, Departamento de Química y Ciencias Ambientales, Laboratorio de Análisis Químico Instrumental (LAQUINS), Escuela Superior Politécnica del Litoral, Guayaquil, Ecuador
[d] Departamento Académico de Química Inorgánica, Facultad de Química e Ingeniería Química, Universidad Nacional Mayor de San Marcos, Lima, Peru
[e] Departamento Académico de Química Analítica e Instrumental, Facultad de Química e Ingeniería Química, Universidad Nacional Mayor de San Marcos, Lima, Peru
[f] Grupo de Química Computacional y Teórica (QCT-UR), Facultad de Ciencias Naturales, Universidad del Rosario, Bogotá, Colombia
[g] Grupo de Química Computacional y Teórica (QCT-USFQ), Instituto de Simulación Computacional (ISC-USFQ), Departamento de Ingeniería Química, Universidad San Francisco de Quito (USFQ), Quito, Ecuador
[h] Centre for Drugs and Diagnostics, Department of Tropical Disease Biology, Liverpool School of Tropical Medicine, Pembroke Place, Liverpool L3 5QA, UK
[i] Universidad del Zulia (LUZ), Facultad Experimental de Ciencias (FEC), Departamento de Biología, Laboratorio de Genética y Biología Molecular (LGBM), Maracaibo 4001, Zulia, Bolivarian Republic of Venezuela
[j] Instituto Venezolano de Investigaciones Científicas (IVIC), Centro de Estudios Botanicos y Agroforestales, (CEBA), Laboratorio de Proteccion Vegetal, 4001 Maracaibo, Bolivarian Republic of Venezuela

ARTICLE INFO

Keywords:
COVID-19
Volume fluctuation
Voronoi
ANM
GNM
Volume Molar

ABSTRACT

The COVID-19 pandemic has accelerated the study of drugs, most notably ivermectin and more recently Paxlovid (PF-07321332) which is in phase III clinical trials with experimental data showing covalent binding to the viral protease M^{pro}. Theoretical developments of catalytic site-directed docking support thermodynamically feasible non-covalent binding to M^{pro}. Here we show that Paxlovid binds non-covalently at regions other than the catalytic sites with energies stronger than reported and at the same binding site as the ivermectin B1a homologue, all through theoretical methodologies, including blind docking. We volumetrically characterize the non-covalent interaction of the ivermectin homologues (avermectins B1a and B1b) and Paxlovid with the mM^{pro} monomer, through molecular dynamics and scaled particle theory (SPT). Using the fluctuation-dissipation theorem (FDT), we estimated the electric dipole moment fluctuations at the surface of each of complex involved in this study, with similar trends to that observed in the interaction volume. Using fluctuations of the intrinsic volume and the number of flexible fragments of proteins using anisotropic and Gaussian elastic networks (ANM+GNM) suggests the complexes with ivermectin are more dynamic and flexible than the unbound monomer. In contrast, the binding of Paxlovid to mM^{pro} shows that the mM^{pro}-PF complex is the least structurally dynamic of all the species measured in this investigation. The results support a differential molecular mechanism of the ivermectin and PF

* Corresponding author.
** Corresponding author at: Instituto Venezolano de Investigaciones Científicas (IVIC), Centro de Estudios Botanicos y Agroforestales, (CEBA), Laboratorio de Proteccion Vegetal, 4001 Maracaibo, Bolivarian Republic of Venezuela.
E-mail addresses: alvaradoysaias@gmail.com (Y.J. Alvarado), lgonzalezpaz@gmail.com (L. González-Paz).

https://doi.org/10.1016/j.compbiolchem.2022.107692
Received 4 January 2022; Received in revised form 28 April 2022; Accepted 2 May 2022
Available online 14 May 2022

homologues in the mM^{pro} monomer. Finally, the results showed that Paxlovid despite beingbound in different sites through covalent or non-covalent forms behaves similarly in terms of its structural flexibility and volumetric behaviour.

1. Introduction

During the COVID-19 pandemic researchers sought new therapeutic approaches to target SARS-CoV-2. A common approach was the repurposing of approved pharmaceutical drugs to reduce costs, risks and time to approval/adoption in clinical settings. Computational methods with a biophysical approach can be used to discover different interactions and relevant drug phenomena that are not considered and are not found during the clinical trial process, especially for existing drugs that could offer a broader medical scope such as ivermectin (Aghdam et al., 2021; González-Paz et al., 2021).

Ivermectin is composed of an approximately 80:20 mixtures of two homologues, avermectin B1a (B1a) and avermectin B1b (B1b), which differ in the presence of a secbutyl and an isopropyl group, at the C25 position, respectively (see Fig. 1). A wide variety of computational biophysical studies have been carried out to determine the capacity of ivermectin to treat COVID-19 due to shown multitarget antiviral activity against SARS-CoV-2 *in vitro* (Koulgi et al., 2021; Azam et al., 2020; Yuce et al., 2021; Choudhury et al., 2021). Ivermectin has shown a higher binding energy to different target proteins of SARS-CoV-2 compared to other antiviral drugs and new candidates, such the alphaketoamide type inhibitor 13b (González-Paz et al., 2021). Many proteins have been suggested to interact with ivermectin, such as the M^{pro} protease which is responsible for most of the post-translational modifications of SARS-CoV-2 polypeptides (Aghdam et al., 2021; González-Paz et al., 2021; Koulgi et al., 2021; Azam et al., 2020). Despite all the efforts made to demonstrate the structural and energetic changes induced in M^{pro} by the binding of ivermectin (González-Paz et al., 2021), the thermodynamic changes that accompany this process from a volumetric perspective still remain unknown. As some authors (Whitten et al., 2005; Chalikian, 2016; Timasheff, 2002) have conclusively demonstrated, this type of study provides information on the role played by hydration in modulating protein stability and its role in ligand binding reactions. It is important to mention that it has been shown that protein-protein and protein-ligand interactions occur with the loss or gain of water molecules around the ligand and/or protein (biological water), a phenomenon with potential pharmacological impact because it is key to the biological activity of these proteins (Chalikian, 2021; Alvarado et al., 2018, 2021; Chalikian and Filfil, 2003; Shek and Chalikian, 2013; Son et al., 2012; Toleikis et al., 2016; Kaur et al., 2018; Sirotkin et al., 2012). Despite the theoretical effort made and the *in vitro* studies of its antiviral activity to date, there are still no experimental reports that confirm the binding and perturbation of M^{pro} by ivermectin. For this reason, we carried out a comparative study of these homologues of ivermectin with the new clinical phase III drug called Paxlovid or PF-07321332 (from here on we will call PF-07321332) of which there is theoretical and experimental data that show its binding to protease M^{pro} in catalytic site (Macchiagodena et al., 2022; Ahmad et al., 2021; Pavan et al., 2021; Vandyck and Deval, 2021; Zhao et al., 2021). Theoretically using directed Docking, a model has been proposed that this binding occurs through a non-covalent binding of PF at the catalytic site causing the formation of the covalently bound species at the site through the formation of a thiolate-imidazolium group (Macchiagodena et al., 2022). Interestingly this species is less thermodynamically favored than the non-covalent complex (Zhao et al., 2021). This study, in addition to being interesting, opens the possibility of evaluating by blind docking the possible formation of complexes with PF-07321332 by thermodynamically favorable non-covalent bonding at sites other than the catalytic site that has been reported (Kneller et al., 2022).

In this study we focus on analyzing the volumetric changes of the structures using the minimum binding energy resulting from blind dockings. Blind docking represents one of the greatest challenges in the field of molecular docking (Agrawal et al., 2019). Blind docking has been described as an unbiased molecular docking approach as it scans the protein structure to locate the ideal ligand binding site, representing a probabilistic approach. However, blind docking represents one of the greatest challenges in the field of molecular docking (Agrawal et al., 2019). In addition, it has been suggested for the study of potential therapeutic agents against coronaviruses (Durojaye et al., 2020).

Despite the limitations of blind docking several tools have been produced such as DockThor which has been been optimized for ligand docking to SARS-CoV-2 targets (Guedes et al., 2021) and has been shown to be relatively successful in situations where the coupling box spans the entire surface of the receiver (Jofily et al., 2021). Especially since, in a virtual screening circumstance, this method has a great advantage: it can determine the best binding pocket for each candidate ligand in a single

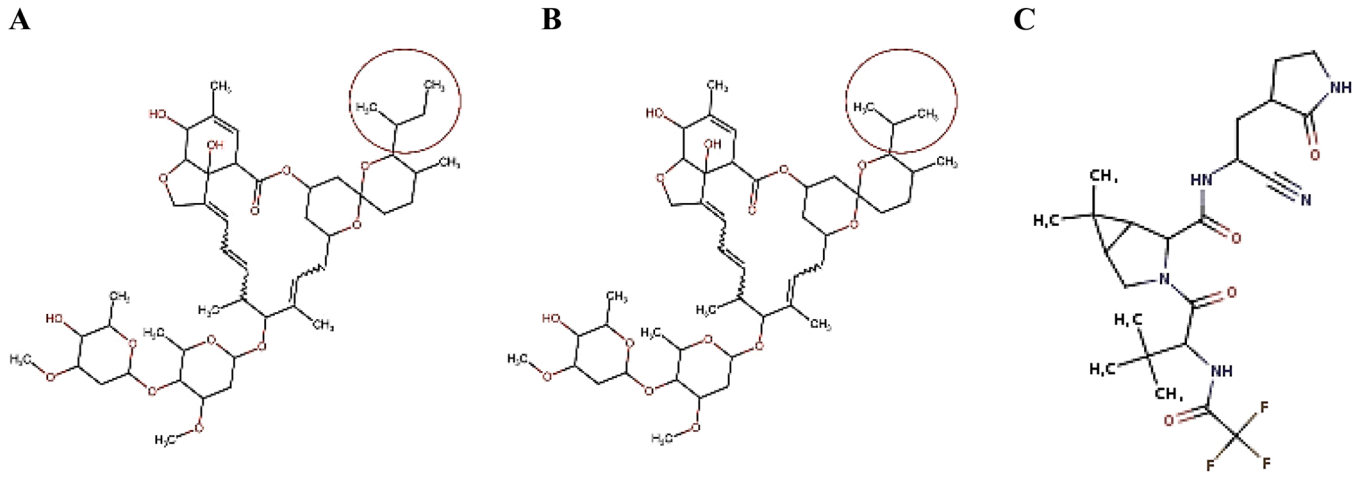

Fig. 1. Molecular structure of the two homologues considered in this study obtained from DrugBank. A) Avermectin B1a (PubChem CID: 6321424), B) Avermectin B1b (PubChem CID: 6321425), C) PF-07321332 (PubChem CID: 155903259). The differential chemical group of each homologues is indicated (for B1a it is secbutyl and B1b is an isopropyl, respectively).

docking run (Jofily et al., 2021).

It has been suggested that although some potent antivirals can bind strongly to the active site, exploring other regions of the protein with the blind docking approach should not be ruled out because a preference for binding to target sites has been demonstrated (Liang et al., 2020). Especially since promising non-covalently bound inhibitors have been reported by applying the molecular docking strategies presented here (Ferraz et al., 2020), and that both covalent and non-covalent binding free energy contributions are important in the binding affinity of an inhibitor towards its target (Awoonor-Williams and Abu-Saleh, 2021).

In addition, it has been suggested that in M^{pro} allosteric inhibition could take place due to the presence of an allosteric site in the protein structure that is not found in the active site. In fact, it is noteworthy that residues such as P122 have been implicated as keys to interactions at the dimer interface and contribute to M^{pro} dimerization (Al Khoury et al., 2022). Interestingly, these residues are part of those involved in the interactions with the homologue B1b and PF-07321332 (non-covalent bonding) described in our study (see supplementary material - Table S1). In light of these observations, we decided to apply the blind docking approach, so as not to exclude the possible inhibition strategies suggested against M^{pro}, such as: (1) interaction with active/catalytic site regions, (2) interaction with allosteric site regions, and (3) interaction with interphase regions associated with enzyme dimer formation (Al Khoury et al., 2022), the latter strategy was the most relevant to our investigation, especially, since M^{pro} is known to depend on homodimerization for its biological activity (Goyal and Goyal, 2020; Tekpinar and Yildirim, 2021).

The volumetric results obtained provide further insight into the possible mechanism by which these drugs inhibit the reaction of formation of the homodimeric protease M^{pro}. For this we build protein-ligand complexes (M^{pro} + avermectin) and (M^{pro} + PF-07321332) on which we have used the Voronoi model implemented in the *3Vee* program (Petřek et al., 2007; Voss and Gerstein, 2010), *HullRad* program (Fleming and Fleming, 2018), the volumetric models proposed by Chalikian et. al (Shek and Chalikian, 2013; Son et al., 2012; Chalikian and Macgregor, 2019) and Graziano-Lee models based in scaled particle theory (SPT) (Graziano, 2006; Lee, 1983; Graziano, 2006; Alvarado et al., 2015). This approach can be translated to other protein-ligand complexes to more accurately determine interactions important for catalysis and the biological activity of these proteins.

In this manuscript we have, for the first time, reported the computational biophysics study of changes induced in the volumetric properties and the hydration of the monomer of the M^{pro} protease (mM^{pro}) and the respective non-covalent complexes formed by binding ivermectin homologues and PF-07321332. In the last section of this paper, a comparative study is also carried out between the non-covalent and covalent complexes thermodynamically more feasible between PF and mM^{pro} detected using blind docking and molecular dynamics.

2. Methodological details

2.1. Building of complexes with docking and molecular dynamics (MD) simulations

The crystal structure of the main protease of SARS-CoV-2 (PDB: 6LU7) was used as it is a key enzyme of coronaviruses and has a fundamental role in mediating viral replication and translation, making it an attractive target for drugs (Panikar et al., 2021; Chhetri et al., 2021). All structures were obtained in PDB format from the RCSB Protein Data Bank (https://www.rcsb.org/). Since the X-ray structure of the PF-07321332-M^{pro} complex is currently available in the Protein Data Bank, and since a covalent bond has already been described, it was considered to study the non-covalent bond as it is a very likely thermodynamic bond. A comparative analysis was performed applying two sampling algorithms (DockThor and AutoDock) for the prediction of compound affinity by detection of covalent and non-covalent binding as suggested for multiple targets including those associated with SARS-CoV-2 (Ferraz et al., 2020; Xavier Senra and Fonseca, 2021). The reported covalent docking was predicted from the AutoDock algorithm's covalent docking approach, which has been validated with various biological systems (Blake and Soliman, 2014; Morris et al., 2009). For this, the enzyme was loaded in the PDB format and the compound of interest was loaded separately as a mol2 file. Subsequently, the binding center was assigned to the frame corresponding to residue Cys145. In addition, the docking calculations were performed following the recommendations of the sampling region of the tests experimentally (Zhao et al., 2021). Predictions of the relative covalent and non-covalent binding energies were made from the sampling algorithm and scoring function offered by AutoDock, and using Molegro Molecular predictions, in order to calculate the contributions of the molecular interactions offered by the tool, such as hydrogen bonds, hydrophobic bonds, electrostatic bonds, and also covalent bonds at the binding site as suggested (Gupta et al., 2015; Mahdian et al., 2021) (see Supplementary material - Table S1). In addition, the non-covalent union was compared with the covalent one after the construction of the covalent model as suggested (Macchiagodena et al., 2022). The X-ray frame of an alpha-ketoamide inhibitor covalently linked to M^{pro} and strictly related (PDB: 7BPR) was used as suggested for the construction of the complex and the comparison between covalent and non-covalent binding of PF-07321332 (Macchiagodena et al., 2022). The homologue structures of avermectin B1a (B1a, CID_6321424) and avermectin B1b (B1b, CID_6321425) that make up ivermectin, as well as the drug PF-07321332 (CID: 155903259) used as a control because it is a reported compound with affinity and inhibitory activity for mM^{pro}, were obtained from PubChem (https://pubchem.ncbi.nlm.nih.gov/) in SDF format and converted to a PDB format using the OpenBabel-3.0 converter (O'Boyle et al., 2011).

The complexes were built in the DockThor-VS web server (https://dockthor.lncc.br/v2/) optimized for the design and reuse of drugs focused on SARS-CoV-2 (see Fig. 2, Fig. 3, Fig. 4, Fig. 5). The DockThor-VS platform utilizes a topology file for the ligand and a specific input file for the protein containing the atom types and partial charges from the MMFF94S force field, and both are generated using the in-house tools MMFF Ligand and PdbThorBox. The file of the ligand is generated by the MMFF Ligand program, which utilizes the facilities of the Open Babel chemical toolbox for deriving partial charges and atom types with the MMFF94S force field, defining the rotatable bonds and the terminal hydroxyl groups, and calculating the properties necessary for computing the intramolecular interactions. In the DockThor program, both protein and ligand are treated with the same force field in the docking experiment. The complexes were built using the flexibility algorithm and blind docking. The affinity prediction and ranking of distinct ligands are performed with the linear model and DockTScore GenLin scoring function. To increase accuracy 30 runs were made with 10^6 evaluations per run. As is usually done, all the water molecules were removed and the PDB files were separated into two different files, one containing the protein and the other containing the ligand structure. All the molecular force field parameterisations were performed automatically by the programs cited. The remaining settings, conditions and parameters offered by the program were used in the default mode (Guedes et al., 2021).

For the prediction of the covalent binding complex, the enzyme predetermined by DockThor was used for the study of M^{pro} and the compound of interest was loaded separately as a PDB file. Subsequently, the binding center was assigned to the frame corresponding to residue Cys145, as has been suggested previously (Xavier Senra and Fonseca, 2021). Similarly, a comparative analysis was carried out between the docking using the scoring functions included in the Molegro Molecular package (MolDock Score, Rank Score and Plants Score). We sought to increase the stringency of the predictions made in this study by using more than one scoring function to determine the best coupled confirmation. In this sense, if most of the scoring functions predict similar

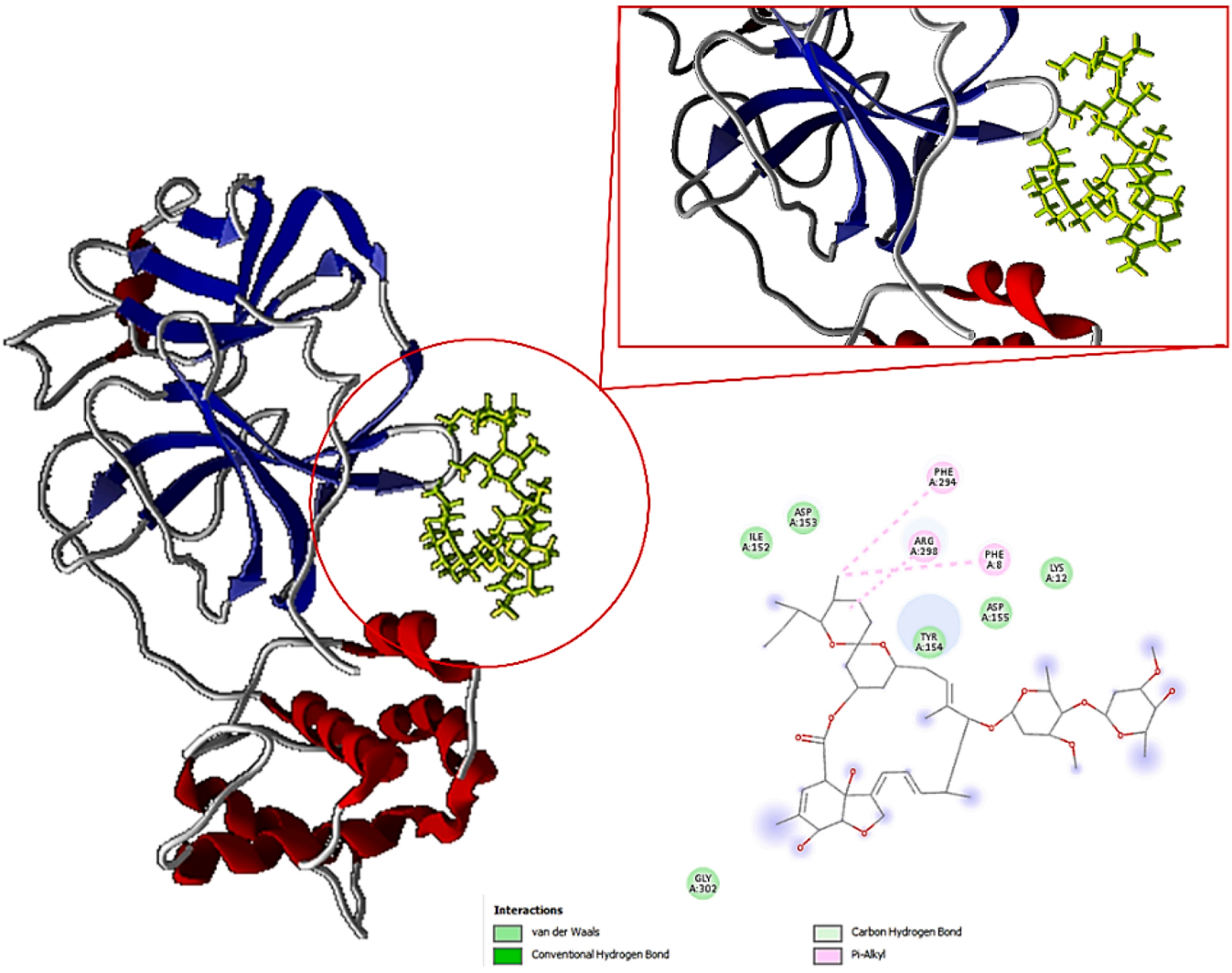

Fig. 2. The most stable conformation of avermectin B1a (PubChem CID: 6321424) is shown in the binding pockets of mM^{pro}. The location and orientation of the B1a structure is indicated in a circle, the closest residues are also shown in the lower right corner. Interactions were predicted from the tool BIOVIA Discovery Studio Visualizer.

trends for the same pose and/or ligand, the energetic mean of various scoring functions could help to optimize the prediction at the probabilistic level and classify the coupled complexes correctly from a set of potential ligand binding conformations and to classify the different conformers based on binding mode (depending on energy score values). In fact, it has been suggested to perform molecular couplings and to apply more than one scoring function like the ones proposed in this study in efforts that consider covalent and non-covalent systems in order to further improve docking accuracy (Blake and Soliman, 2014; Saikia et al., 2014). Overall, predicting differences in covalent and non-covalent binding free energy contributions for inhibitors could be a plausible explanation for their *in vitro* differences in antiviral activity as observed in *in vitro* assays. This indicates that covalent and non-covalent binding free energy contributions are important in the binding affinity of an inhibitor towards its target (Awoonor-Williams and Abu-Saleh, 2021). Therefore, other authors have applied more than one scoring method for the selection of the most promising candidates during covalent and non-covalent bonding molecular dockings (Delre et al., 2020) (see **Supplementary material -** Table S1).

It is important to note that even though the interactions presented in the 2D diagram appear weaker than the reported relative coupling energies, non-covalent free energy contributions are important in the binding affinity of an inhibitor towards its target as has been reported (Awoonor-Williams and Abu-Saleh, 2021) In addition, the 2D diagrams were made from BIOVIA Discovery Studio Visualizer and by way of illustration they show a limited number of interactions. In this sense, to compensate for the limitations of the visualizers in predicting the nature of the interactions involved, a search was made for the residues and the interactions involved using the tools BIOVIA Discovery Studio Visualizer and Molecular Molecular Visualizer (see **Supplementary material -** Table S1).

Simulations were performed for docking to sample the minimum energy conformations and validate if there was a structural and conformational alteration of the mM^{pro} complexes, as well as the stability of the ligand binding (see Fig. 6). For a protein-ligand complex, the MD system went through three phases: the relaxation phase, the equilibrium phase (composed of two equilibrium runs), and the production phase for sampling the trajectories of interest as suggested previously (Xavier Senra and Fonseca, 2021; Mahdian et al., 2021; Patel et al., 2012; Grahl et al., 2021; Gautam et al., 2019; Madhavi et al., 2021; Yonezawa, 2013). MD simulation of crystal structures was carried out in an explicit water system. Specifically, the solvation of the system was performed in an 8.0 Å solvation box. Our MD system also consisted of one copy of each protein system and one copy of the docking ligand. An Amber99SB-ILDN force field was applied to the complex with the TIP3P water model. Ions were added to the system proportionally both to

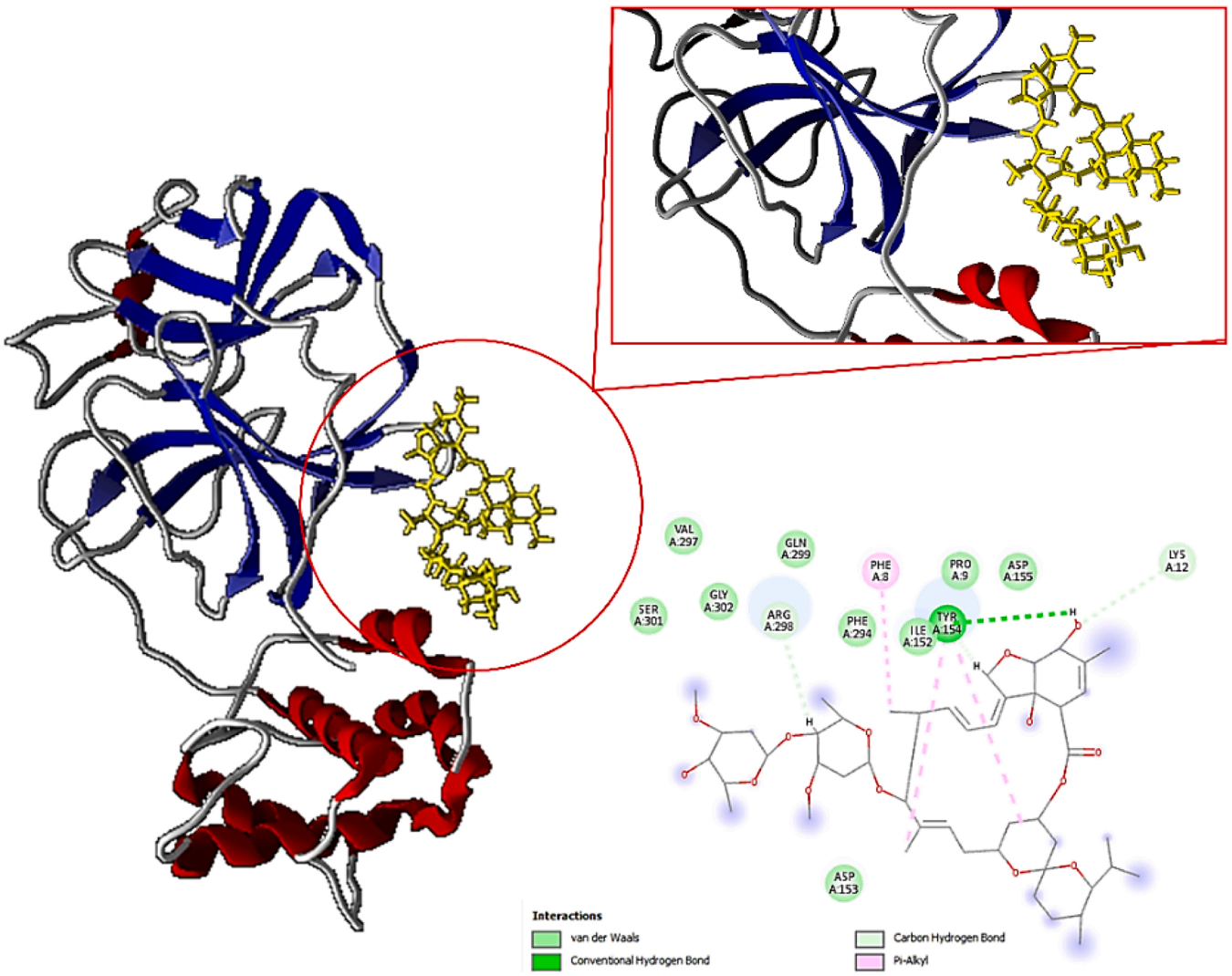

Fig. 3. The most stable conformation of avermectin B1b (PubChem CID: 6321425) is shown in the binding pockets of mM^{pro}. The location and orientation of the B1b structure is indicated in a circle, the closest residues are also shown in the lower right corner. Interactions were predicted from the tool BIOVIA Discovery Studio Visualizer.

neutralize the overall net charge and to simulate the physiological condition of 0.15 M. Na+ ions were selected for the cationic contribution, while Cl− ions were selected for the anionic effect. Periodic boundary conditions were applied and Berendsen's algorithm was adopted to perform molecular docking at constant temperature and pressure (300 K and 1 atm).

For this, after initially applying the simulation method based on the steepest descent (5000 steps) and then the conjugate gradient energy minimization method (5000 steps) with position restrictions on the atoms of the protein-ligand complex, it was carried out modeled in an initial 100 ps simulation with the positions of the atoms in the protein-ligand complex constrained by a force constant of 10 kcal/(mol*Å2) to allow water molecules to diffuse around the protein and reach equilibrium with the protein-ligand system. All water molecules in the model were treated as rigid bodies, allowing for a simulation time step of 2 fs. The Particle Mesh Ewald (PME) method was used to calculate the electrostatic contribution to non-bonded interactions with a cutoff of 14.0 Å and a time step of 1 fs. In protein systems, TIP3P water is suitable for the PME. The cutoff distance of the Van der Waals interaction was 14.0 Å. After applying the steepest descent algorithm to meet the energy minimization of all systems, the canonical NVT set was applied for 100 ps balanced of all systems and thermalized at 300 K. This was followed by a second run of 100 ps on the isothermal-isobaric NPT set to equilibrate the system at 1 atm and 300 K and progressively drive the equilibrium of each system. The SHAKE algorithm (used to satisfy link geometry constraints) was applied to the system and the time step was set to 2 fs. Finally, the production step was performed with the output of the NPT set, which was used as the initial configuration of an MD production series at a constant temperature of 300 K for a total simulation time of 100 ns. Minimum energy structures in PDB format were obtained every 10 ns as target structures extracted from a 100 ns trajectory to be used in the following analyses. All MD simulations and additional adjustments were performed using cosgene/myPresto. Cosgene/myPresto which is available at https://www.mypresto5.jp/en/ (González-Paz et al., 2021, 2020; González-Paz et al., 2021, 2020; Kasahara et al., 2020).

In this sense, we worked with each of the avermectin homologues (B1a and B1b) and showed these molecules establish a thermodynamically favorable ($\Delta G \approx -10$ kcal/mol) and stable docking with mM^{pro} with an RMSD $\approx \leq 4$ Å, noting that a minor fluctuation of the mM^{pro} + B1b complex was predicted. The relative binding energy of the PF-07321332 control was $\Delta G \approx -8$ kcal/mol showing stable binding with mMpro as expected (RMSD $\approx \leq 4$ Å) (see Fig. 6).

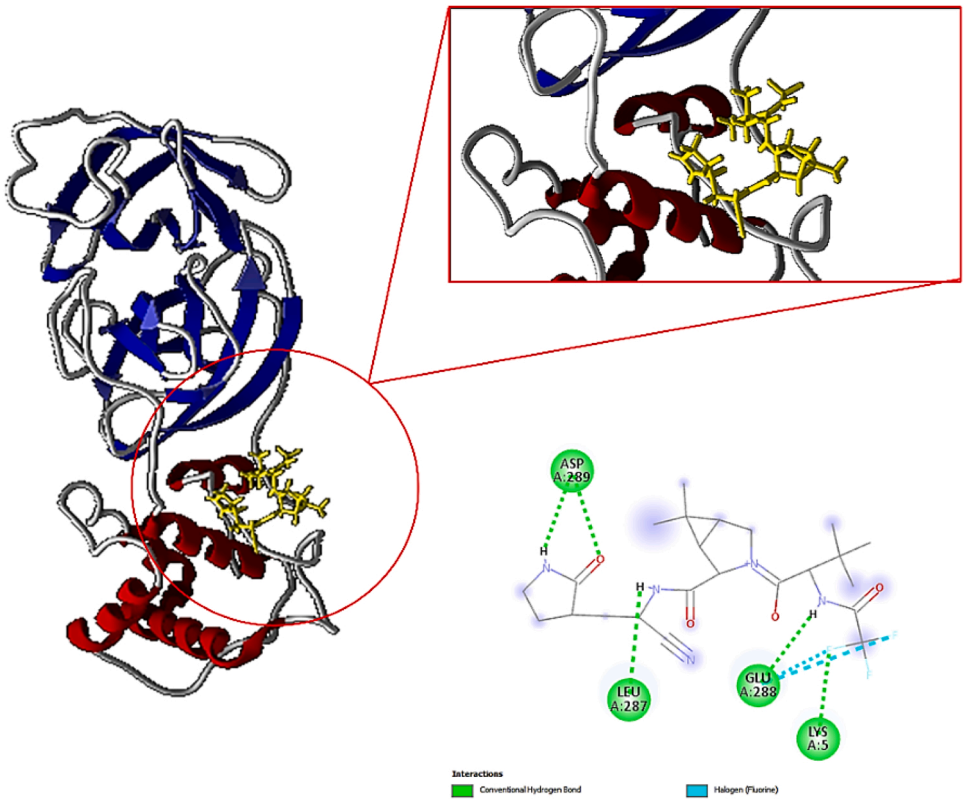

Fig. 4. The most stable conformation of PF-07321332 (PubChem CID: 155903259) is shown in the binding pockets of mM^{pro}. The location and orientation of PF-07321332 structure is indicated in a circle; the closest residues are also shown in the lower right corner. Interactions were predicted from the tool BIOVIA Discovery Studio Visualizer.

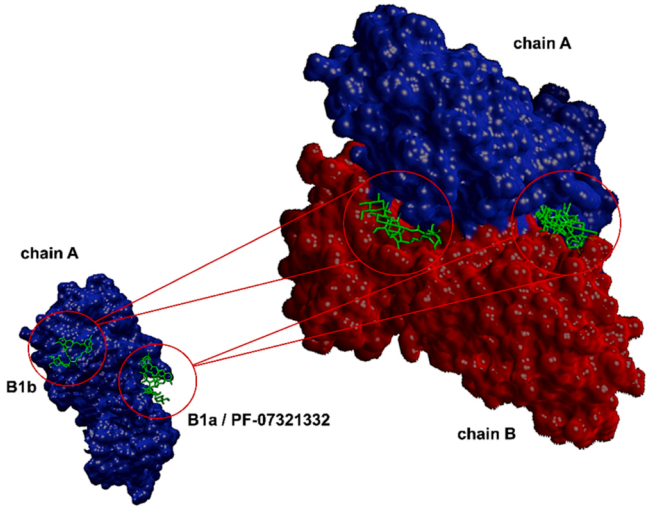

Fig. 5. The most stable conformation of the avermectins and PF-07321332 is shown in the binding pockets of the dimeric M^{pro} protein (dM^{pro}). The location and orientation of each structure is indicated in a circle.

3. Theory

The partial molar volume of protein V_p by definition (Alvarado et al., 2018, 2015; Chalikian and Filfil, 2003; Graziano, 2006) is considered to be constituted of two volumetric contributions, a molecular or geometric contribution V_m (volume of van der Waals V_w and volume of internal voids V_v) and a non-intrinsic contribution $\langle\Theta\rangle_{ni}^{m}$ (volumetric contribution from repulsive v_T and attractive interactions V_{int}):

$$V_p = V_m + \langle\Theta\rangle_{ni}^{m} + \beta_T^o RT \quad (1)$$

$$V_m = V_w + V_v \quad \text{and} \quad \langle\Theta\rangle_{ni}^{m} = V_T + V_{int} \quad (2)$$

$$V_p = V_w + V_v + V_T + V_{int} \quad (3)$$

V_w is the van der Waals volumes of all the protein constitutive atoms of protein and V_v is volume of cavities within the protein from imperfect atomic packing, dependent of temperature, proportional to molar mass M_0, and equal to the geometric volume of protein impenetrable to surrounding solvent molecules (Chalikian and Filfil, 2003; Shek and Chalikian, 2013; Son et al., 2012; Toleikis et al., 2016; Kaur et al., 2018; Alvarado et al., 2021; Chalikian and Macgregor, 2019; Chhetri et al., 2021). While the thermal volume V_T (by definition is a quantity positive, i,e, > 0) is the empty volume around of protein which is due to the mutual protein-solvent vibrations, intermolecular packing or steric effect, and the interaction volume V_{int} (by definition is a quantity negative, i, e, < 0) represents reduction of the solvent volume under the influence of direct specific and non-specific solute-water interactions (attractive interactions) (Alvarado et al., 2018, 2015; Chalikian and Filfil, 2003; Shek and Chalikian, 2013; Son et al., 2012; Chalikian and Macgregor, 2019; Voloshin et al., 2015). The last term in the Eq. 1 is the ideal volumetric contribution and generally is neglected due their low magnitude ($\beta_T^o RT \approx 1 cm^3/mol$) in comparison with the magnitude of V_p of proteins.

Alternatively, the scaled particle theory (SPT) defines partial molar volume of a solute as:

$$V_p = V_C + V_{int} \quad (4)$$

Where V_C is the cavity volume that hosts the solute and by definition is $V_C = V_m + V_T$ Chalikian and Macgregor (2019); Patel et al. (2012);

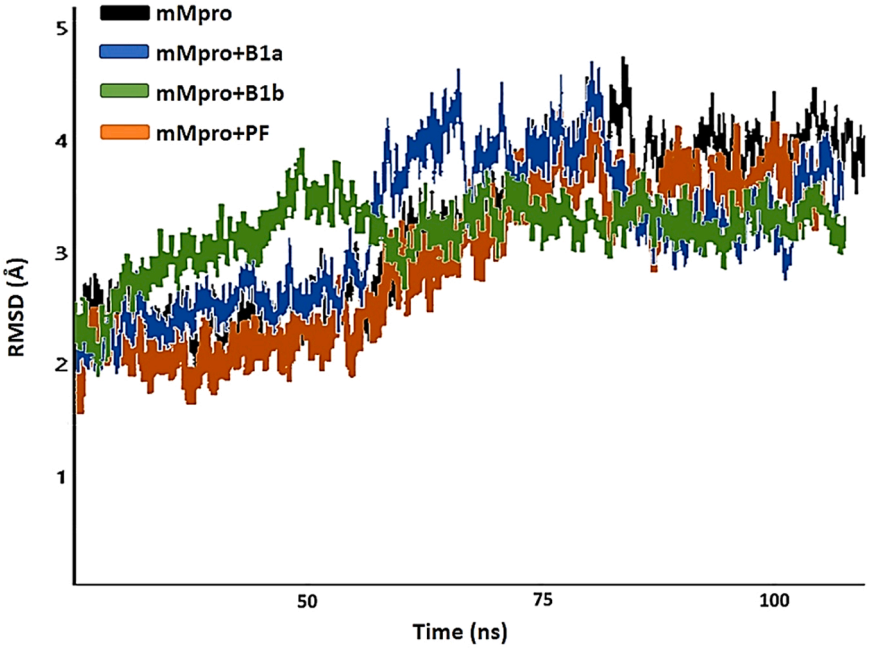

Fig. 6. The Root Mean Square Deviations (RMSD) of Cα relative to the starting frame during 100 ns MD simulation. mM^{pro} is shown in the presence and absence of each homologue (B1a and B1b), and PF-07321332. The trajectories represent the mean of two simulation cycles at 100 ns for each case.

Mejía-Tamayo et al. (2018); Kharakoz (1992). In the SPT model proposed by Lee-Graziano (Graziano, 2006; Lee, 1983; Graziano, 2006; Alvarado et al., 2015), the cavity volume V_C of solute in a binary mixture of hard spheres can be estimated as

$$V_C = \left(y^3 + 3Ay^2 + 3A^2y + A^2B\right)\left(\frac{V_w^0}{C}\right) \tag{5}$$

Where $y = \frac{r_m}{r_w}$, r_m is the hard sphere radious of molecule protein (Patel et al., 2012) and $r_w = 1.4$ Å is the hard sphere radious of solvent water molecule, $A = \frac{(1-\xi)}{(1+2\xi)}$, $B = \frac{(1-\xi)}{\xi}$, $C = \left(1+3A+3A^2+BA^2\right)$, $\xi = 0.380$ is the volume packing density of solvent (water) at 298 K, and v_w^0 is molar volume of water as solvent. This equation can be translated into a simpler expression

$$V_C = V_m + V_T \tag{6a}$$

$$V_m = \frac{4\pi}{3} k_m N r_m^3 \tag{6b}$$

Here N is avogradrós number. According to this theory the repulsive component V_T depends on the molecular size of solute and solvent, and packing density of water as proposed by Lee (Lee, 1983), Graziano (Graziano, 2006; Graziano, 2006) and by us (Alvarado et al., 2015) through calculations in aqueous medium. It is important to mention that this geometric model for small nonpolar molecular systems gives values very close to the Pierotti-Kharakoz thermodynamic model for V_T Alvarado et al. (2015); Kharakoz (1992).

$$V_T = 4\pi k_v N r_m^2 \Delta_p + 4\pi k_v N r_m \Delta_p{}^2 + \frac{4\pi}{3} k_v N \Delta_p^3 \tag{7}$$

Here $\Delta_p = Ar_w$ is the thickness of a layer of empty volume surrounding the solute molecule (protein). In this model (Eqs. 6 and 7) the constant $k_m = k_v = 1$ for small nonpolar systems (Voss and Gerstein, 2010; O'Boyle et al., 2011) as was originally proposed by Lee and Graziano. For proteins we have found that $k_m = 1.7$ and $k_v = 2.4$ for proteins (see supplementary material Table S2 and S3). There is another approximate expression for V_T proposed by Chalikian and Mcgregor (Chalikian and Macgregor, 2019).

$$V_T = S_A \Delta_p \tag{8}$$

Where S_A is solvent accessible surface area of protein and Δ_p as defined in the Eq. 7.

It is important to mention that this model although descriptive, has limitations due to the difficulty of exactly separating the border between the surface of the protein and the solvent (interfacial region). This model has been very useful to understand important processes such as hydration/dehydration of proteins involved in protein-ligand binding, protein-protein binding and chemical-induced unfolding (Alvarado et al., 2018; Shek and Chalikian, 2013; Son et al., 2012; Chalikian and Macgregor, 2019; Voloshin et al., 2015; Mejía-Tamayo et al., 2018; Aggarwal and Biswas, 2020).

In computational biophysics studies, the molecular volume in a fluid is determined using the Voronoi-Delaunay model and this amount is 15% larger than the molecular volume V_m previously defined in Eq. 1 and 2 (Filfil et al., 2004). This thermodynamic quantity is equivalent to the volume of a cavity dry or anhydrous (know as Voronoi volume) (Voloshin et al., 2015) in solution where the protein molecule has been placed (Chalikian and Macgregor, 2019; Voloshin et al., 2015; Filfil et al., 2004). This anhydrous volume will be defined herein after as V_p^{nh} of protein, which strictly and by definition, is equal to

$$V_p^{nh} = V_w + V_M^{empty} + V_B^M \tag{9}$$

where V_M^{empty} is the internal void volume of protein and V_B^M is the part of boundary empty space assigned to the solute (Voloshin et al., 2015). If we assume that the protein-water interface division is the same in both models, then the three first components of the volumetric Eq. 3, and geometric equation 6 based in molecular dynamics can be empirically approximated as

$$V_p^{nh} = V_w + V_M^{empty} + V_B^M \cong V_w + V_v + V_T = V_m + V_T = V_C \tag{10}$$

And the partial molar volume of a protein can then be written as [see Eqs. (3) and (9)]

$$V_p = V_p^{nh} + V_{int} \tag{11}$$

The volume of interaction V_{int} is the only term of $\langle\Theta\rangle_{ni}^{m}$ that contains information about the redistribution of water molecules between the hydration shell and bulk phase (Son et al., 2012; Chalikian et al., 1996). On the other hand, in molecular dynamics (Voloshin et al., 2015; Voloshin et al., 2015) the contribution V_{int} is defined as the difference between the volume of the hydration shell around of solute V_{hyd} and the occupied volume $\frac{n_{hyd}}{\rho_0}$ in the bulk by the same number of water molecules (Voloshin et al., 2015; Voloshin et al., 2015; Brovchenko et al., 2010).

$$V_{int} = V_{hyd} - \frac{n_{hyd}}{\rho_0} \tag{12}$$

Or alternatively

$$V_{int} = V_p - V_p^{nh} \tag{13}$$

If in the Voronoi–Delaunay approach, the border is defined as the Voronoi surface of the solute molecule, the Eqs. 12 and 13 are equivalent. Also, the fact that in volumetric studies the term V_{int} has an analog definition to Eq. 12 is very interesting.

$$V_{int} = n_w\left(V_w^s - V_w^0\right) \tag{14}$$

Where the number of water molecules around of protein is n_w, V_w^s is the partial molar volumes of hydration and bulk water, respectively (Son et al., 2012; Chalikian and Macgregor, 2019). Therefore, the empirical Eq. 11 is a good approximation. In fact, recent studies have shown that $\langle\Theta\rangle_{ni}^{m}$ and $V_B^M + \Delta V$ are equal (Voloshin et al., 2015).

In the high dilution regime the thermodynamic theory leads to the following expression for the partial molecular volume of proteins (Richards, 1993)

$$V_p = V_{nh} + M_p\delta_h\left(v_w^h - v_w^0\right) \tag{15}$$

Where V_{nh} is the dry volume of protein (here it is approximated to the Voronoi volume (V_p^{nh})), M_p is the dry molar mass of protein, v_w^h is the specific volume of bound water to the protein molecule and v_w^0 is the specific volume of nearby water. Chalikian and co-workers (Kaur et al., 2018) have proposed that $v_w^h - v_w^0 = -0.09\frac{cm^3}{g}$, while δ_h is the amount of grams of water associated with the protein per gram of protein, it is a measure of the degree of hydration of protein and it does not depend on temperature and concentration of solute (Richards, 1993; Monkos, 2013, 2004).

A comparison of Eqs. 11 and 15 shows that the second term in both equations is:

$$V_{int} = M_p\delta_h\left(v_w^h - v_w^0\right) \tag{16}$$

In hydrodynamic studies (Richards, 1993; Monkos, 2013, 2004) the volume of a particle in solution is called hydrodynamic volume V_h and contains two components, one corresponding to the partial molar volume of the dry protein (also defined here as V_p^{nh} to maintain the same nomenclature) and the other due to volume of the hydration layer V^{sh} Richards (1993); Monkos (2013).

$$V_h = V_p^{nh} + V^{sh} \tag{17}$$

$$V^{sh} = M_p\delta_h v_w^h \tag{18}$$

Eq. 15 is very useful for theoretically estimating δ_h if V_h and V_p^{nh} are known.

$$\delta_h = \frac{\left(V_h - V_p^{nh}\right)}{M_p v_w^h} \tag{19}$$

Then, evaluating the change induced in each of the contributions to the components V_m and $\langle\Theta\rangle_{ni}^{m}$ of apparent molar volume in the protein-ligand binding reactions provides important information on the structural and hydration changes that the protein undergoes in biological processes.

The proteins are dynamic molecules (Lindow et al., 2013; Marchi, 2003), and at thermal equilibrium, the intrinsic volume V_p^{nh} (geometric component) and the hydration or interaction volume V_{int} are constantly fluctuacting around their mean values $\left\langle V_p^{nh}\right\rangle$ and $\langle V_{int}\rangle$ Lindow et al. (2013); Marchi (2003); Dadarlat and Post (2001); Kharakoz and Sarvazyan (1993); Pfeiffer et al. (2008); Mori et al. (2006); Persson and Halle (2018). The structural dynamic is very important for biological function of protein and stability (Marchi, 2003; Persson and Halle, 2018; Paul et al., 2017; Reid et al., 2021; Tang and Dill, 1998; Tang and Kaneko, 2020; Kapoor and Winter, 2016; Rother et al., 2003; Jiang et al., 2014; Cooper, 1984). The intrinsic protein flexibility is relevant to interaction with ligand and can contribute to the binding process (Mori et al., 2006; Persson and Halle, 2018; Luong et al., 2015; Gekko and Hasegawa, 1986; Zhang et al., 2015; Barletta et al., 2019; Barletta and Fernández-Alberti, 2018). The internal cavities play an important role on structural flexibility of protein (Mori et al., 2006; Rother et al., 2003; Jiang et al., 2014; Barletta et al., 2019; Barletta and Fernández-Alberti, 2018; Pereira et al., 2006; Stank et al., 2016). Studies support that protein binding processes occur with important changes in the fluctuation of the volume of the internal cavities and surface hydration of protein (Lindow et al., 2013; Marchi, 2003; Dadarlat and Post, 2001; Kharakoz and Sarvazyan, 1993; Pfeiffer et al., 2008; Mori et al., 2006; Persson and Halle, 2018; Reid et al., 2021; Kapoor and Winter, 2016; Gekko and Hasegawa, 1986). Statistical thermodynamic theory states that if V_p^{nh} and V_{int} fluctuate independently of each other then the intrinsic volume fluctuaction is possibly related thermodynamically with intrinsic compressibility (Mori et al., 2006; Cooper, 1984) as:

$$\beta_T^I = \frac{\left\langle\delta V_I^2\right\rangle}{KTV_I} \tag{20}$$

Where $\left\langle\delta V_I^2\right\rangle$ is the mean square intrinsic volume fluctuaction, V_I is the intrinsic volume of protein, K is the Boltzmann contant, T the absolute temperature, and β_T^I the isothermal intrinsic compressibility coefficient. The mean square intrinsic volume fluctuaction can be statistically estimated from $V_{i(j)}$ values and mean value of V_i obtained from dynamic molecular simulation as:

$$\left\langle\delta V_I^2\right\rangle = \frac{1}{N}\sum_{j=1}^{n}\left(V_{I(j)} - \langle V_I\rangle\right)^2 \tag{21}$$

Then $\left\langle\delta V_I^2\right\rangle$ is a quantitative measure of protein dynamics. However, in many studies the amount used for comparative studies is:

$$\left\langle\delta V_I^2\right\rangle^{1/2} = \sqrt{\frac{1}{N}\sum_{j=1}^{n}\left(V_{I(j)} - \langle V_I\rangle\right)^2} \tag{22}$$

On the other hand, Fornés proposed an attractive phenomenological model based on the Fluctuation-Dissipation Theorem (FDT) that allows estimating the thermal fluctuations of the electric dipole moment in units of the water molecule dipole moment $\delta\mu_r$ on the surface of the protein from the hydrodynamic molecular volume V_h^m Fornés (2008).

$$\delta\mu_r = \frac{\left\langle\delta\mu_p^2\right\rangle^{\frac{1}{2}}}{\mu_w} = \frac{\sqrt{\frac{V_h^m}{3}(4\nu - 1)KT}}{1.84} \tag{23}$$

Where $V_h^m = \frac{V_h}{N}$, $\nu \geq 2.5$ is the Simha factor and $\mu_w = 1.84$ D is the water molecule permanent electrical dipole moment. Fornés observed that the electric dipole moment fluctuations $\delta\mu_r$ as a function of the molecular weight ranged from 15 to 115, increasing with the size of the protein molecule.

As the hydrodynamic volume V_h, Simha factor ν and anhydrous volume V_p^{nh} (Voronoi volume) can be estimated using different meth-

odologies such as *HullRad* (Fleming and Fleming, 2018) and *3Vee* programs (Petřek et al., 2007; Voss and Gerstein, 2010), all parameters described here in this section can be calculated for the monomer of the M^{pro} protease (mM^{pro}) and their respectives non-covalent complexes formed by binding ivermectin homologues and PF-07321332 in physiological medium. *HullRad* (https://hullrad.wordpress.com/) is an open source algorithm to calculate hydrodynamic parameters of biomolecules. It works for folded proteins, intrinsically disordered proteins and protein complexes. This method uses a convex hull model to estimate the hydrodynamic volume of the molecule and is orders of magnitude faster than common methods (Fleming and Fleming, 2018). *3Vee*, can automatically extract and comprehensively analyze all the internal volumes from protein structures. It rapidly finds internal volumes by taking the difference between two rolling-probe solvent-excluded surfaces, one with as large as possible a probe radius and the other with a solvent radius (typically 1.5 Å for water) (Petřek et al., 2007; Voss and Gerstein, 2010).

For comparison purposes only, graphs of the spatial envelope simulated with the *WAXSiS* server (http://waxsis.uni-goettingen.de/) of the monomer M^{pro} in the presence and absence of each of the homologues were incorporated. WAXSiS runs a short explicit-solvent MD simulation using YASARA. After the simulation has finished, a spatial envelope is constructed that includes the biomolecule and its solvation shell at a distance of 7 Å from the biomolecule atoms. The excluded-solvent scattering is computed based on a pure-water simulation that was conducted previously. The WAXSiS model allows to detect changes in global protein parameters, such as the radius of gyration, the multimeric state, aggregation or changes in the solvation shell from a molecular dynamics simulation in solution. This makes it possible to trace the conformational transitions of the complexes on a small scale and allows accurate measurements at wider angles due to the effect of the ligands, and their effect even at the level of the solvation shell. For more details of the WAXSiS method we recommend reviewing (Knight and Hub, 2015; Chen and Hub, 2014).

For the prediction of the number of flexible fragments (N_f), *HingeProt* was used, a web server to predict rigid protein parts and the flexible hinge regions that connect them in the native protein chain topology using elastic network models (EN). *HingeProt* uses Gaussian lattice models (GNM) and anisotropic lattice models (ANM) (http://bioinfo3d.cs.tau.ac.il/HingeProt/) (González-Paz et al., 2021; Emekli et al., 2008).

4. Results and Discussion

4.1. Comparative analysis between volumetric properties of monomeric M^{pro} (mM^{pro}) and their non-covalent complexes formed by binding of homologues of ivermectin homologues and PF-07321332 in physiological medium

From a volumetric point of view the formation of complex by protein binding a ligand can be analyzed from the change in partial molar volume of protein ΔV_p according to:

$$\Delta V_p = \Delta V_p^{nh} + \quad \Delta V_{int} \tag{24}$$

Where $\Delta V_p = V_p(complex) - V_p(monomer)$ is the difference in V_p between the mM^{pro}-ligand complex and the ligand-free M^{pro} monomer. The ligands studied are the homologues of ivermectin (B1a and B1b) and PF-07321332. The term ΔV_p^{nh} is the change in the Voronoi volume of proteins and ΔV_{int} is the change in the interaction volume. In the following sections, we will analyze the volumetric changes obtained in each of the contributions ΔV_p^{nh} and ΔV_{int} as well as of each of their components to the partial molar volume of protein.

4.1.1. Changes induced in Voronoi volume $\mathbf{V_p^{nh}}$ by non-covalent binding of ivermectin and PF-07321332 to the M^{pro} monomer (mM^{pro})

Table 1 shows the values of Voronoi Volume obtained by molecular dynamic (MD) simulations. A simple inspection reveals that the anhydrous volume V_p^{nh} is higher in magnitude when the monomer is in complex with the B1b homologue (from here forward called mM^{pro}-B1b) in comparison to the ligand-free monomer (mM^{pro}), the monomeric complex mMpro-PF and mM^{pro}-B1a. This gives the order obtained as mM^{pro}-B1b > mM^{pro} > mM^{pro}-PF ≈ mM^{pro}-B1a. The difference ΔV_p^{nh} between mM^{pro}-B1b and mM^{pro} was + 93.35 cm^3/mol, − 136.70 cm^3/mol between the complex mM^{pro}-B1a and mM^{pro}, and − 133.08 cm^3/mol for the complex mM^{pro}-PF. Although these amounts may seem small, they are indeed significant. Volumetric changes involved in folding or unfolding induced in proteins by ligand binding are very modest (Chalikian and Filfil, 2003; Shek and Chalikian, 2013; Son et al., 2012, 2014; Alvarado et al., 2021; Filfil et al., 2004; Son and Chalikian, 2016; Chalikian and Breslauer, 1996; Kaur et al., 2021). According to Eq. (10) the change in the Voronoi volume can be calculated as:

$$\Delta V_p^{nh} = \Delta V_w + \Delta V_v + \Delta V_T \tag{25}$$

If the change in the van der Waals volume is considered negligible $\Delta V_w \approx 0$ (Son et al., 2014), then the difference in ΔV_p^{nh} is due to binding-induced changes in the volume of the internal cavities ΔV_v of the mM^{pro} and the contribution of volume that comes from the repulsive protein-water interactions ΔV_T [see Eqs. (6–8) and (25)]. It is important to mention that the ΔV_p^{nh} values are excellently reproduced by Eqs. 6 and 7 of the Lee-Graziano SPT model. In fact, the difference ΔV_C between mM^{pro}-B1b and mM^{pro} was + 115.19 cm^3/mol, − 120.68 cm^3/mol between the complex mM^{pro}-B1a and mM^{pro} and − 84.50 cm^3/mol between the complex mM^{pro}-F and mM^{pro} Which establishes that V_C is close to V_p^{nh} and maintains that the approximations involved in this work are adequate.

With this in mind, we can suggest that $\Delta V_p^{nh} \approx \Delta V_v + \Delta V_T$, and making use of the values obtained for V_T from SPT model (see Table 1 and Eqs.7 or 8) we find that $\Delta V_T = -11.29\ cm^3/mol$ for the difference between the mM^{pro}-B1b complex and the mM^{pro}, a value of $\Delta V_T = -27.39$ cm^3/mol for the difference between the mM^{pro}-B1a complex and mM^{pro} and $\Delta V_T = -56.54$ cm^3/mol for the difference between the mM^{pro}-PF complex and mM^{pro}. The negative value of ΔV_T in all cases reflects the decrease of surface areas within the ligand-protein interfaces Chalikian and Filfil, 2003. As the complex mM^{pro}-PF exhibits

Table 1
Volumetric properties obtained from the minimum energy structures at 100 ns of the M^{pro} monomer (mM^{pro}) and the mM^{pro}-B1a, mM^{pro}-B1b and mM^{pro}- PF non-covalent complexes formed by the union of the ivermectin homologues (B1a and B1b) and PF-07321332.

	V_p^{nh}	V_h	V_m	V_T	V_{int}	$\langle\Theta\rangle_{ni}^{m}$	V_p	V_v	δ_h
mM^{pro}	26960.49	44431.81	23929.08	3031.41	-1727.93	1303.48	25232.56	4443.09	0.57
mM^{pro}–B1a	26823.79	43762.61	23819.77	3004.02	-1675.27	1328.75	25148.53	4333.78	0.55
mM^{pro}–B1b	27053.84	47025.24	24033.62	3020.22	-1975.19	1045.03	25078.64	4547.63	0.65
mM^{pro}–PF	26827.41	44139.10	23852.54	2974.87	-1712.15	1262.72	25115.26	4366.55	0.56

Volume quantities expressed in cm^3/mol; δ_h in $g_{water}/g_{protein}$; van der Waals volume of mM^{pro} (V_w): 19485.99 cm^3/mol estimated with 3*Vee* model using probe test of 0 *Å*.

the largest decrease in surface it becomes clear that the magnitude of ΔV_p^{nh} is dominated by the change in the volumetric component ΔV_v. This result is very interesting because it allows us to suggest that the value of ΔV_p^{nh} comes from changes in the size distribution of the internal cavities of the monomer induced by binding of homologues of ivermectin and PF-07321332 due to the small magnitude of ΔV_T in comparison with ΔV_v. It is important to note that this change in the volumetric component V_v in the mM^{pro} monomer is different in the complexes with B1a and PF-07321332 (dVv < 0 in both cases) instead of B1b and PF-07321332 (dVv < 0 in both cases). It is important to mention that the magnitude of V_v depends on the conformational state of the protein (Chalikian and Filfil, 2003). These volumetric results at 100 ns are in agreement with the results obtained by molecular simulations using Anisotropic Network models (ANM) and Gaussian Network Model (GNM) (González-Paz et al., 2021; Emekli et al., 2008). In the ANM and GNM, if the number of flexible fragments N_f of a protein-ligand complex is higher than in the respective uncomplexed protein in its native state, it is interpreted that an unfolding induced by the ligand occurred, otherwise, if they decrease in protein-ligand complex in relation to the protein without ligand binding, compaction or refolding is said to have occurred (González-Paz et al., 2021; Emekli et al., 2008). In Fig. 7, a similar trend is observed but with a number of flexible fragments that differs between the complexes at the end of 100 ns. The number of flexible fragments N_f of complexes suggest the differential behavior of the threes ligands (B1a, B1b and PF-07321332) when they bind to the mM^{pro}. Interestingly, the homologue B1b induced unfolding while homologue B1a and PF-07321332 induced structural compaction in the mM^{pro} (see Fig. 7).

It should be mentioned that homologues of ivermectin interact to the mM^{pro} at different sites as shown in Fig. 2, Fig. 3, Fig. 4 and Fig. 5. While the ligand PF-07321332 bind in the same site that the homologue B1a in the M^{pro} monomer (see Fig. 5).

This previous analysis was possible due to the knowledge of the Voronoi volume V_p^{nh} and the thermal volume V_T for each protein involved in this analysis. While in the case of the second term ΔV_{int} of Eq. (24), we must first determine the hydration volume V^{sh} and ΔV^{sh} from the hydrodynamic volume V_h and Voronoi volume of each species. Once V^{sh} is known, it is possible to determine δ_h and then estimate both V_{int} and ΔV_{int} in each case.

4.1.2. Changes induced in the hydrodynamic volume $\mathbf{V_h}$ and the volume of the hydration layer $\mathbf{v^{sh}}$ by non-covalent binding of ivermectin and PF-07321332 in M^{pro} monomer (mM^{pro})

The values obtained for the hydrodynamic volume are shown in Table 1. The same pattern as that observed for the Voronoi volume is observed *i.e.* mM^{pro}-B1b > mM^{pro} > mM^{pro}-PF > mM^{pro}-B1a. The difference in V_h between mM^{pro}-B1b, mM^{pro}-B1a and mM^{pro}-PF complex with mM^{pro} were ΔV_h = + 2593.43, − 669.20 cm^3/mol, and − 292.71 cm^3/mol, respectively. A look at Eq. 17 shows that $\Delta V_h = \Delta V_p^{nh} + \Delta V^{sh}$, and so $|\Delta V^{sh}| \gg |\Delta V_p^{nh}|$ is true for the homoloques of ivermectin, in contrast, in the case of mM^{pro}-PF the value of ΔV^{sh} is only slightly larger than ΔV_p^{nh}. After this, the change in the volume of the monomer hydration layer dominates. This result is very interesting because it establishes that the volume of the hydration layer V^{sh} is very different in the three complexes in relation to the native monomer, ful filling that V^{sh}(mM^{pro}-B1b) 19971.40cm^3/mol > V^{sh}(mM^{pro}) 17471.32cm^3/mol > V^{sh}(mM^{pro}-B1a) 17311.69cm^3/mol > V^{sh}(mM^{pro}-B1a) 16938.62cm^3/mol . Therefore, ΔV^{sh}(mM^{pro}-B1b - M^{pro}) = + 2500.08 cm^3/mol, ΔV^{sh}(mM^{pro}-B1a - Mpro) = − 532.70 cm^3/mol and ΔV^{sh}(mM^{pro}-PF - Mpro) = − 159.63 cm^3/mol. That is, the hydration layer in the monomer is thicker when it binds to the B1b homologue than when it binds to the B1a homologue or PF-07321332, while this layer is thinnest in the monomer when it binds to the homologue B1a. These results suggest that the ivermectin homologues and PF-07321332 affect the monomer's dimerization reaction to form the dimeric M^{pro} (dM^{pro}), a process which is important for viral replication (Goyal and Goyal, 2020; Marchi, 2003; Macchiagodena et al., 2022; Ahmad et al., 2021; Pavan et al., 2021; Vandyck and Deval, 2021; Zhao et al., 2021). It is very interesting to see that PF-07321332 and B1a dehydrate mM^{pro} as The hydration layer of the proteins known as biological water has been associated as a fundamental part of the protein and which plays an important role in the biological function of proteins (Ball, 2017; Laage et al., 2017; Adhikari et al., 2020).

Additional information about the changes induced in the hydration of the proteins was obtained from the degree of hydration measured as grams of water per gram of monomer δ_h, which was calculated with Eq. 19 and the values of the hydrodynamic volume V_h and Voronoi volume V_p^{nh} (see Table 1). The results obtained are shown in Table 1. The mM^{pro} is more hydrated compared to the native mM^{pro} when bound to the B1b

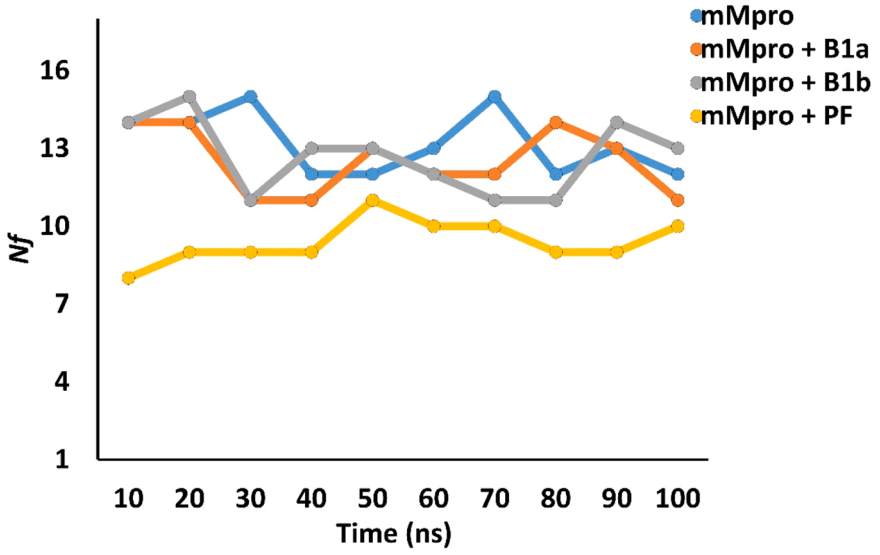

Fig. 7. Comparison between the fluctuation of the number of flexible fragments $\left\langle \delta N_f^2 \right\rangle^{1/2}$ of non-covalent complexes using Anisotropic Network models (ANM) and Gaussian Network Model (GNM). The predictions correspond to the minimum energy structures at 100 ns MD simulation.

homologue. In comparison, the monomer is less hydrated compared to the mMpro-B1a complex, mMpro-PF complex and the native mM^{pro} from a hydrodynamic point of view. That is, the B1a homologue and PF-07321332 induced loss of water molecules in the mM^{pro} upon being bound. These δ_h values are interesting as they provide information on the degree of hydration in the monomer and its change during complex formation by ligand binding. However, the information on the contraction of the hydration layer mediated by attractive interactions that come from the water-surface interactions of the protein is obtained through the V_{int} volumetric component.

Another relevant aspect to highlight from these δ_h results is that the hydration obtained for the mM^{pro} (δ_h = 0.57) is equal to the value reported for lysozyme (δ_h = 0.57) and close to porcine elastase (δ_h = 0.53) using other proteases models (Fornés, 2008). In fact, this degree of hydration is high and any change in this can significantly affect the molecular recognition events for this protease, since it is known that for this type of biochemical reaction in proteins, hydration is an extremely important driving force (Chalikian, 2021). It is very important to note there are no reports of this type of data for proteases associated with SARS-CoV-2 and in particular for M^{pro}.

4.1.3. *Changes induced in the interaction volume* $\mathbf{V_{int}}$ *by non-covalent binding of homologues of ivermectin and PF-07321332 in* M^{pro} *monomer* (mM^{pro})

The interaction from the specific and non-specific van der Waals forces of water as a solvent with the polar, non-polar and charged surface residues of the protein is quantified in the attractive volumetric contribution V_{int} (see Eqs. 14 and 16) to the partial or apparent molar volume V_p. This volumetric quantity V_{int} therefore is a measure of the contraction of the volume of water as a solvent in the proximity of the charged, and polar groups of the protein (Son et al., 2012; Chalikian and Macgregor, 2019; Alvarado et al., 2015; Aggarwal and Biswas, 2020). Hence its importance to evaluate the induced changes in protein hydration due to ligand binding. Table 1 shows the values obtained for this volumetric property, demonstrating the following trend $V_{int}(mM^{pro}\text{-B1b}) > V_{int}(mM^{pro}) \approx V_{int}(mM^{pro}\text{-PF}) > V_{int}(mM^{pro}\text{-B1a})$.

The difference ΔV_{int} between mM^{pro}-B1b and mM^{pro} is $-247.26\ cm^3/mol$, $+52.66\ cm^3/mol$ between mM^{pro}-B1a and mM^{pro} and $+15.78\ cm^3/mol$ between mM^{pro}-PF and mM^{pro} These results suggest that the binding of ivermectin B1b to mM^{pro} induces a redistribution of the charged and polar surface groups, favoring the exposure and the population of these to the solvent. While in the case of the complex mM^{pro}-B1a and PF-07321332, the exposure of these surface amino acid residues is disfavored and the exposure of the nonpolar ones could be favored, which possibly affects the solubility of the protein as occurs with hydrophobic solutes that tend to aggregate in water (Graziano, 2016, 2017). It is important to see the consistency of these results by remembering that B1a and PF-07321332 bind at the same site within the protein mM^{pro}. In any case, the little water that surrounds the protein or the site where B1a or PF-07321332 are bound should be dispersed or poorly structured. Thus affecting the degree of local hydration could be important. It has been proposed that water plays an important role in the catalytic site in M^{pro} (Macchiagodena et al., 2022). These results are also important since depending on which region this hydration or dehydration occurs in the protein, the flexibility, stability and mechanisms of recognition of the protein can be significantly affected (Voloshin et al., 2015; Marchi, 2003; Persson and Halle, 2018; Tang and Dill, 1998; Tang and Kaneko, 2020). The homodimerization of this monomer to form the biologically active species could also be affected (Goyal and Goyal, 2020). In this direction, the results obtained are interesting as the negative value of ΔV_{int} observed for the formation of the mM^{pro}-B1b complex is associated with a high hydration which suggests lower aggregation tendency, diminution in hydrophobicity and higher charge surface in proteins (Aggarwal and Biswas, 2020). In contrast, in the case of homologue B1a and PF-07321332, the formation of the mM^{pro}-B1a complex leads to a positive value of ΔV_{int} which is associated with low hydration and as consequence a higher aggregation tendency or an increased tendency to form aggregates or disordered clusters (an increase in hydrophobicity and lower charge in surface of proteins) (Aggarwal and Biswas, 2020). In any case, the results suggest the negative effect on the homodimerization reaction. It is very important to mention that these results support the reports of the inhibition of the dimerization reaction of mM^{pro} by binding of the PF-07321332 drug (Macchiagodena et al., 2022; Ahmad et al., 2021; Pavan et al., 2021; Vandyck and Deval, 2021; Zhao et al., 2021). Therefore, as PF-07321332 and B1a bind at the same site, it is possible to propose that this ivermectin homologue has a similar effect.

It is very interesting that the trend observed for V_{int} was similar to obtained for the electric dipole moment fluctuations on the surface (see Eq.23) of the protein mM^{pro}-B1b ($\delta\mu_r$ = 55.7) > mM^{pro} ($\delta\mu_r$ = 54.2) = mM^{pro}-PF ($\delta\mu_r$ = 54.2) > mM^{pro}-B1a ($\delta\mu_r$ = 54.1), suggesting that this electrical property plays an important role on the contraction of the first hydration layer, perhaps by affecting the water-water dipole interactions at the protein-water interface (Seyedi and Matyushov, 2018). It should also be noted that the values obtained for $\delta\mu_r$ are in the expected order for a protein with a mass of 33.4 kDa (Fornés, 2008).

The value of the mM^{pro}-B1a complex is 0.18% lower than that obtained for mM^{pro} and mM^{pro}-PF complex while it is 2.87% lower when compared to the mM^{pro}-B1b complex. Although these percentages appear to be very small, there are no other reports of comparative studies between protein-ligand complexes and free protein that allow an analysis of this situation. It is clear that more studies on this topic are necessary. However, these small differences between $\delta\mu_r$ makes sense if it is thought to be related to changes in the populations of exposed polar amino acid residues on the surface of the protein by binding to ivermectin homologues and PF-07321332, and it is expected that these polar residue populations change by only a small fraction during global conformational changes.

These results, together with those obtained for δ_h and V_{int}, suggest that each protein-ligand complex must have a difference both in the thickness of the hydration layer and in the distribution of the water molecules on the protein. Figs. 8 and 9 demonstrate the differences in the layers of hydration, particularly in the distribution of the water molecules in the surface cavities of each species. In the case of Fig. 8, the 3Vee model allows estimation of the radius of the hydration layer (thickness of water layer) from the surface of the protein, estimating the distance to be 10 $\AA$ as $\Delta r_w = r_p^w - r_p^{nh}$, where r_p^w is the radius from the center of the protein to its surface plus a distance of 10 $\AA$ from this surface and r_p^{nh} is the intrinsic or Voronoi radius of protein, both amounts. r_p^w and r_p^{nh} have been estimated from the respective volumes. The results give the following trend Δr_w(mMpro) 14.76 $\AA$ ≈ Δr_w(mMpro-B1b) 14.75 $\AA$) > Δr_w(mMpro-PF) 13.30 $\AA$ > Δr_w(mMpro-B1a) 12.98 $\AA$. It is clear that the mMpro-B1a complex is the least hydrated of all the proteins, while the mMpro-B1b complex has a hydration close to or equal to the native protein.

4.1.4. *Changes induced in the non-intrinsic volume contribution to partial molar volume* $\mathbf{V_p}$ *of non-covalent complexes in physiological medium*

Graziano reported that the non-intrinsic volumetric contribution $\langle\Theta\rangle_{ni}^{m}$ at infinite dilution in water for mixture of hard spheres is always a small and positive quantity (Graziano, 2006). We have recently confirmed this for model globular proteins (Alvarado et al., 2018, 2015). This is because this contribution to V_p is the result of a balance between the repulsive volumetric component V_T and the attractive component V_{int} [see Eq. 2], and always dominates V_T. In this study the values obtained for $\langle\Theta\rangle_{ni}^{m}$ using the data of V_T and V_{int} are shown in Table 1, giving the following trend $\langle\Theta\rangle_{ni}^{m}(mM^{pro}\text{-B1b}) < \langle\Theta\rangle_{ni}^{m}$ (mM^{pro}-PF) $< \langle\Theta\rangle_{ni}^{m}$ (mM^{pro}) < $\langle\Theta\rangle_{ni}^{m}$ (mM^{pro}-B1a). This is most easily seen in numerical form like $\Delta\langle\Theta\rangle_{ni}^{m}$ (mM^{pro}-B1b - mM^{pro}) = - 238.82 cm^3/mol, $\Delta\langle\Theta\rangle_{ni}^{m}$ (mM^{pro}-PF

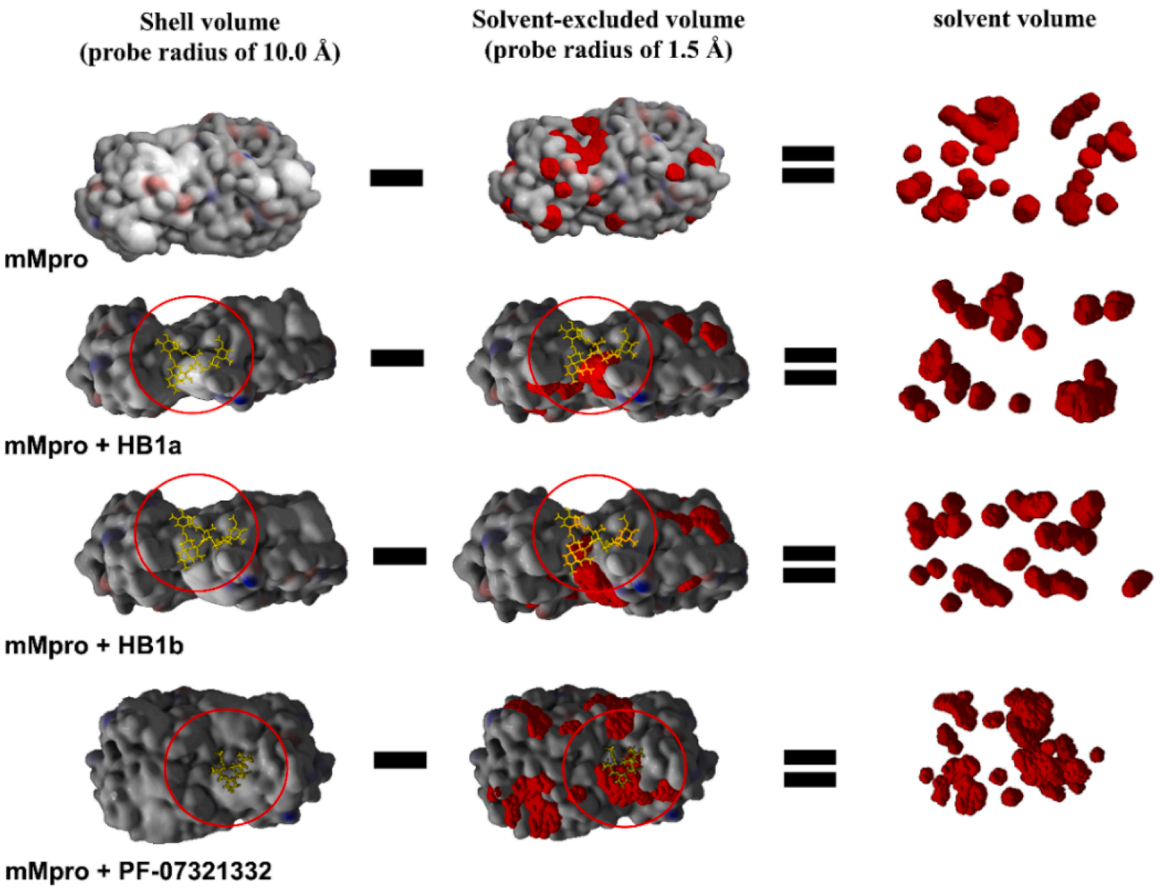

Fig. 8. Comparison between the volume of solvent extracted from mM^{pro} in the presence and absence of each homologue and PF-07321332 using the *3vee Solvent Extraction Module* (http://3vee.molmovdb.org/solventExtract.php).

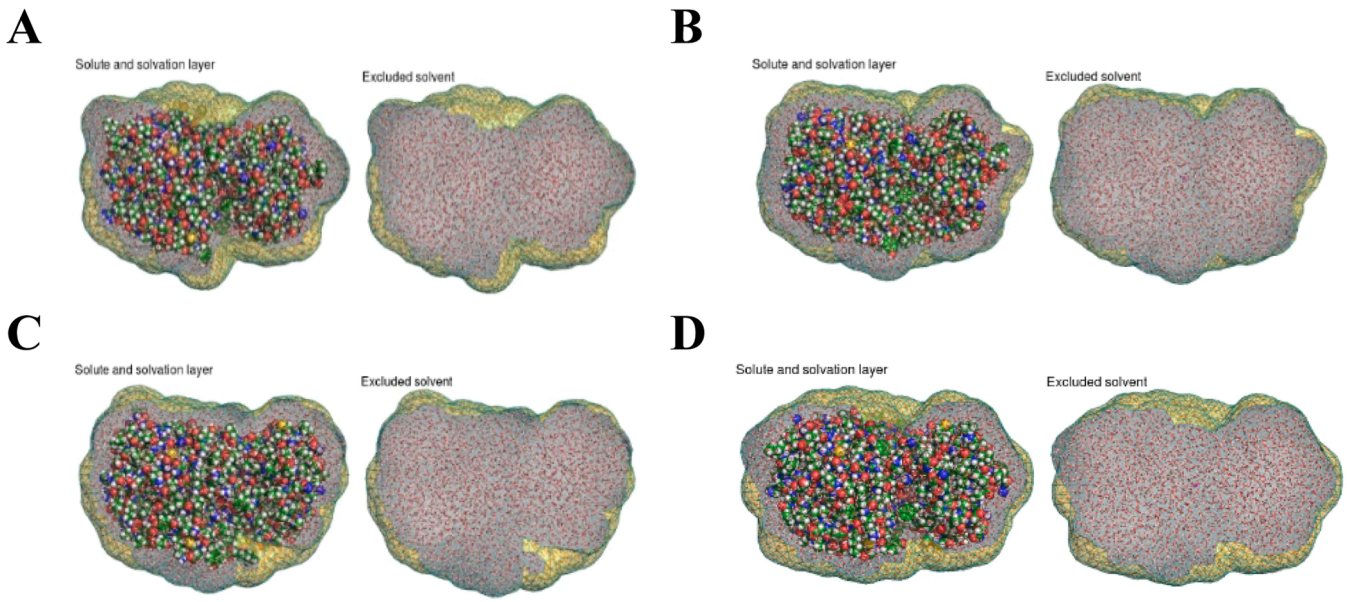

Fig. 9. Comparison between the simulated spatial envelope with WAXSiS server of mM^{pro} in the presence and absence of each homologue (http://waxsis.uni-goettingen.de/). A, mM^{pro} free; B, mM^{pro} + Avermectin B1a (B1a); C, mM^{pro} + Avermectin B1b (B1b); D, mM^{pro} + PF-07321332. The predictions correspond to the minimum energy structure at 100 ns MD simulation. The simulated spatial envelope includes the biomolecule and its solvation layer at a distance of 7 Å from the atoms of the biomolecule.

- mMpro) = - 40.76 cm^3/mol and $\Delta\langle\Theta\rangle_{ni}^{m}$ (mM^{pro}-B1a - mM^{pro}) = + 40.29 cm^3/mol. The difference in the sign of this parameter is due to the fact that in the two firsts cases where $\Delta\langle\Theta\rangle_{ni}^{m} < 0$, the repulsive volumetric component water-protein V_T dominates in the unbound monomer, while in the last case this repulsive component dominates in the complex, which reflects that the mechanism involved in the volume change for the formation of the complexes is different in each case. It is interesting to note that although data suggest the B1a homologue and PF-07321332 bind in the same site in mM^{pro} (see Fig. 5), the property $\Delta\langle\Theta\rangle_{ni}^{m}$ has a similar magnitude but a different sign.

4.1.5. Changes induced in the partial molar volume $\mathbf{V_p}$ of non-covalent complexes in physiological medium

Based on Eq. 11 and using the data for Voronoi volume V_p^{nh} and interaction volume V_{int} of Table 1, we have determined the partial molar volume in physiological medium of mM^{pro}, the mM^{pro}-B1a, mM^{pro}-B1b and mM^{pro}-PF complexes. In the same table the values obtained for this property are shown following the trend, *i.e.* V_p (mM^{pro}) > V_p (mM^{pro}-B1a) > V_p (mM^{pro}-PF) > V_p (mM^{pro}-B1b). The homologues of ivermectin and PF-07321332 induced a decrease in apparent molar volume V_p of mM^{pro} with ΔV_p (mM^{pro}-B1b - mM^{pro}) = - 153.91 cm^3/mol, ΔV_p (mM^{pro}-PF - mM^{pro}) = - 117.30 cm^3/mol and ΔV_p (mM^{pro}-B1a - mMpro) = - 84.03 cm^3/mol. It is important to note that although in all cases ΔV_p has negative sign, the mechanism involved in the partial molar volume V_p change is different in each case. For the mM^{pro}-B1b complex, the change in volume ΔV_p is dominated by the attractive component ΔV_{int}. That is, the attractive interaction of the charged and polar groups on the surface of the protein with the water molecules (hydration layer). While in the case of the mM^{pro}-B1a and mM^{pro}-PF complex, the change in ΔV_p is dominated by the ΔV_p^{nh} component, which is dominated by changes in the distribution of size of the internal cavities of the monomer ΔV_v. Then we can clearly see with these results with the structure of minimum energy at 100 ns that the change in the volumetric properties of the mM^{pro} induced by the ivermectin homologues proceeds by different mechanisms. But the volumetric changes induced in mMpro by B1a and PF-07321332 proceed by the same mechanism.

The results obtained with the structure of minimum energy at 100 ns for the formation of the complexes involve a conformational change that is reflected volumetrically in the ΔV_v component and in ΔV_{int} as expected theoretically and experimentally, so our results are consistent. Although our results seem only qualitative, we can see that similar information is obtained if the analysis is made in the traditional manner using the empirical model proposed by Chalikian and co-workers (Chalikian and Macgregor, 2019). Additionally, the methodology here used was achieved by estimating the thickness of the thermal volume $\Delta_p = \left(\frac{V_p^{nh} - V_m}{S_A}\right)$ from the solvent accessible surface area S_A and thermal volume $V_T = \left(V_p^{nh} - V_m\right)$ as suggested by the empirical model of Chalikian and collaborators. Our values estimated in each case were ~ 0.5 Å, which is in the range reported in the literature (1–0.5 Å) (Patel et al., 2012; Kharakoz, 1992). Although lower values are also known (Chalikian and Macgregor, 2019). Graziano has argued that the value should be 0.5 Å (Graziano, 2013).

The analysis presented here is important from a biophysical chemical perspective to understand the changes induced in the monomeric protein M^{pro} by binding of ivermectin homologues and PF-07321332. The change in volume observed is mainly attributed to the components V_{int} in the case of homologue B1b, and V_v in the cases of homologue B1a and PF-07321332 drug. This suggest that for B1b binding the contraction of solvent volume may have the greatest effect on the change in volume. Whereas, for B1a and PF-07321332 binding the volume of cavities within the protein may have the greatest effect on the change in volume.

4.2. Behaviour dynamic of the partial molar volume $\mathbf{V_p}$ and Voronoi Volume of non-covalent complexes

As previously discussed, the volumetric component contributing the most to ΔV_p in B1a/mM^{pro} and PF/mM^{pro} is the cavity volume or internal voids V_v, whereas the interaction volume V_{int} at 100 ns is the major contribution to ΔV_p in the case of B1b/mM^{pro}. Moreover, the geometric component V_v is within of intrinsic volume $V_p^{nh} = V_I$, while V_{int} contributes in V_p balancing V_p^{nh}.

By analyzing the data presented in Table 2 using Eq. 22 for the case of intrinsic or Voronoi volume and protein volume, it is possible to estimate the mean square of the volume fluctuation in each case ($\left\langle \delta V_p^2 \right\rangle^{1/2}$ or $\left\langle \delta V_I^2 \right\rangle^{1/2}$). The accuracy of Eq. 22 depends on several factors, one of which is having a significantly large number of structures (snapshots) of the protein of interest being studied by molecular dynamics. We performed a comparative study between the results obtained for staphylococcal nuclease (SNase) (Voloshin et al., 2015) with 5000 structures (snapshots) at 50 ns and our methodology using 10 structures at 100 ns. Through it, we have found to be able to reproduce the fluctuation of the protein volume $\left\langle \delta V_p^2 \right\rangle^{1/2}$ and the intrinsic or Voronoi volume $\left\langle \delta V_I^2 \right\rangle^{1/2}$. If in Eq. 22 we consider a statistical correction factor of $K_s = 0.57$ associated to this protein, *i.e*:

$$\left\langle \delta V_i^2 \right\rangle^{1/2} = K_s \sqrt{\frac{1}{N}\sum_{j=1}^{n}\left(V_{i(j)} - \langle V_i \rangle\right)^2} \; i = I \text{ or } P \tag{26}$$

with this equation we estimate the fluctuation of the intrinsic volume using the Voronoi volume ($V_I = V_p^{nh}$, *see Table2*). By considering that this represents the geometry volume inaccessible to the solvent, then in terms of $\left\langle \delta V_I^2 \right\rangle^{1/2}$, we obtained the following trend: mM^{pro}-B1b (218.74 cm^3/mol) > mM^{pro}-B1a (197.47 cm^3/mol) > m^{Mpro} (175.11 cm^3/mol)

Table 2
Molar volume V_p and Voronoi volume V_p^{nh} values for the monomer and its non-covalent complexes with the ivermectin homologues and PF-07321332 in a time range of 10–100 ns.

Time (ns)	Voronoi volume (cm3/mol)				Molar volume (cm3/mol)			
	mM^{pro}	mM^{pro}–B1a	mM^{pro}–B1b	mM^{Pro}-PF	mM^{pro}	mM^{pro}–B1a	mM^{pro}–B1b	mM^{Pro}-PF
10	26540.76	27298.93	27327.84	26911.11	24620.19	25315.27	25338.34	25186.35
20	26718.41	26742.5	26684.08	26705.76	24886.94	24807.33	24749.51	25108.24
30	26361.31	26343.24	26227.01	26357.09	24586.37	24621.61	24539.6	24567.74
40	27046.61	26949.05	27206.19	27051.43	25225.53	25172.51	25348.04	25339.7
50	26739.49	26632.3	26863.54	26770.8	24954.09	24991.07	25028.79	25076.83
60	26201.72	26274.59	26348.66	26273.38	24558.1	24662.71	24656.52	24722.66
70	27086.96	27091.77	27233.89	27013.49	25233.07	25392.32	25253.24	25304.16
80	26734.67	26782.85	26909.31	26682.88	24919.69	25110.14	25071.43	24987.2
90	26236.65	26177.63	26355.28	26246.28	24555.11	24653.62	24669.85	24683.19
100	26960.49	26823.79	27053.84	26827.41	25232.56	25148.53	25078.64	25115.26

and > m^{Mpro}-PF (160.29 cm^3/mol). This result establishes that both complexes with ivermectin (B1a and B1b) are more dynamic and/or flexible than the native monomer, while the mM^{pro}-B1b complex is more dynamic than the mM^{pro}-B1a complex. However, the mM^{pro}-PF complex is the least dynamic or flexible of all molecular species.

In the case of $\left\langle \delta V_p^2 \right\rangle^{1/2}$ the results obtained were 160.78 cm^3/mol (mM^{pro}-B1b), 153.84 cm^3/mol (mM^{pro}), 152.95 cm^3/mol (mM^{pro}-B1a) and 143.86 cm^3/mol (mM^{pro}-PF). The corresponding values of $\left\langle \delta V_p^2 \right\rangle^{1/2}$ are in the 30–200 cm^3/mol range previously reported (Persson and Halle, 2018). The mM^{pro}-B1a complex and the mM^{pro}-PF complex are 0.6% and 7% less dynamic than the native monomer, respectively, while the mM^{pro}-B1b complex is 4.5% more dynamic than the native monomer. Thus, the fraction of volume fluctuaction $\frac{\langle \delta V_p^2 \rangle^{1/2}}{V_p}$ in all cases was around 0.6%, which is close to that reported for other smaller proteins than mM^{pro} (34.5 kDa) (Mori et al., 2006; Persson and Halle, 2018). Nonetheless, it is twice the mean value reported for a larger set of proteins that includes proteins of greater mass than mM^{pro} (Gekko and Hasegawa, 1986). It is very interesting to see that the complexes with the smallest volume fluctuation ($\left\langle \delta V_p^2 \right\rangle^{1/2}$, *e.g.*, the mMpro-PF and mMpro-B1a complexes, also have the lowest V_{int} values.

Since V_{int} is a measure of the shrinkage of the hydration layer due to the attractive interactions of the protein surface groups with water molecules, and since the major contribution comes from the presence of charged groups exposed on the protein surface to the solvent (Shek and Chalikian, 2013; Son et al., 2012), then the fraction of charged groups in these complexes should be low compared to the monomer. Therefore, the interfacial tension γ_{pw} between the protein and water, must be high relative to the native monomer. The opposite is true for the mM^{pro}-B1b complex, which exhibits the highest structural dynamics and the highest V_{int} value of all species, suggesting a high fraction of charged surface groups exposed to water. Accordingly, we can expect a lower protein-water interfacial tension of all values. It should be noted that a low value of γ_{pw} is associated with a high degree of protein hydration and *vice versa*, being in agreement with the adhesive-cohesive model for protein compressibility, in which the attractive forces of water compete with the intraprotein interactions favoring folding proposed by Dadarlat and Post (Dadarlat and Post, 2001).

To support this idea, we estimate the interfacial tension γ_{pw} using the value of $\left\langle \delta V_p^2 \right\rangle^{1/2}$ and the average radius of the protein $\langle r_p \rangle$ (see Table 1) and the model proposed by Lee(Lee, 1983).

$$\gamma_{pw} = \frac{KT}{2\varpi} \tag{27}$$

Here, $\varpi = \frac{\langle \delta V_p^2 \rangle^{1/2}}{\langle r_p \rangle}$ and $\langle r_p \rangle = \sqrt[3]{\frac{3V_p}{4\pi N}}$, the results obtained showed the following trend for $\gamma_{pw}(cal/mol^{-1}/\AA^{-2})$, mM^{pro}-PF(γ_{pw} = 26.7) > mM^{pro}-B1a(γ_{pw} = 25.1) > mM^{pro} (γ_{pw} = 24.9) > mM^{pro}-B1b(γ_{pw} = 23.8), which supports what was previously discussed.

Therefore, the results obtained in this work showed that $\left\langle \delta V_p^2 \right\rangle^{1/2}$, V_{int}, γ_{pw} and δ_h are correlated and agree with the Dadarlat-Post model (Dadarlat and Post, 2001). This model suggests also that high compressibility, resulting from large fluctuations in the molecular volume of the protein, corresponds to an enthalpically less stable protein (Dadarlat and Post, 2001). Another possible connection may come from the inverse relationship between protein flexibility and stability (Tang and Dill, 1998; Kamerzell and Middaugh, 2008). Moreover, it has been reported that the hydration of a protein is favored as its rigidity increases (Remsing et al., 2018). Based on these arguments, we propose that the mM^{pro}-B1a and mM^{pro}-PF complexes are more enthalpically stable than the unbound monomer, whereas the mM^{pro}-B1b complex, is enthalpically unstable with respect to the native monomer.

The values of $\left\langle \delta V_I^2 \right\rangle^{1/2}$ are of higher magnitude and have a different trend than the values of $\left\langle \delta V_p^2 \right\rangle^{1/2}$ revealing the important contribution that the fluctuation of the hydration layer has in V_p and does not contribute in V_p^{nh}. An interesting result was obtained by estimating the number of flexible N_f fragments of each biomolecule between 0 and 100 ns (see Fig. 9) using ANM+GNM methods (González-Paz et al., 2021; Emekli et al., 2008). The values obtained for the fluctuation of the number of flexible fragments $\left\langle \delta N_f^2 \right\rangle^{1/2}$ with these data had the same trend [mM^{pro}-B1b (1.42) > mM^{pro}-B1a (1.27) > mM^{pro} (1.23) > mM^{pro}-PF (0.84)] as that obtained for the fluctuation of the Voronoi volume $\left\langle \delta V_I^2 \right\rangle^{1/2}$. That is, the order in the structural flexibility correlates with the order in the structural dynamics.

We propose that the increase or decrease in monomer structural dynamics induced by PF-07321332 or ivermectin binding has some inhibitory effect on homodimer formation (Macchiagodena et al., 2022; Ahmad et al., 2021; Pavan et al., 2021; Vandyck and Deval, 2021; Zhao et al., 2021). As demonstrated, complex formation involves a change in volume fluctuation. It is also observed that this change correlates with changes in hydration, internal cavity distribution, interfacial tension and enthalpy stability, since some of these factors play an important role in relevant biological processes such as biological recognition. It is interesting to consider that these volumetric and thermodynamic properties depend on the binding site in the monomer. For example, the similarity in mechanism between PF-07321332 and the B1a homologue that bind at the same site, compared to the different mechanism evidenced for B1b that binds at a different site in the monomer. If one further considers that due to the binding site, all the ligands involved here may sterically block protein-protein binding to form the homodimeric protein based on the dimeric structure displayed in PDB: 6LU7. So, given the evidence of inhibitory effect on M^{pro} by PF-07321332, our results suggest that ivermectin derivatives should also have some effect.

4.3. Comparative study of the covalent and non-covalent complex of PF-07321332 with mM^{pro}: dynamic behavior of the Voronoi volume V_p^{nh} and the number of flexible fragments N_f

PF-07321332 ligand is known to bind covalently at the catalytic site of M^{pro} (Zhao et al., 2021), theoretical studies using directed docking suggest that this occurs by a two-stage process. The first involves the formation of a non-covalent complex at the same site and followed by an electrophilic coupling between the thiol group of a cysteine at the catalytic site and the nitrile group from the PF-07321332 a forming a thio-imidazolium bond giving stability to the covalent complex (Macchiagodena et al., 2022). Although the covalently linked species is thermodynamically less stable than the non-covalent complex, this covalent complex is the only species detected so far (Zhao et al., 2021). This covalent complex indicates that the blocking of the catalytic site is its main disturbing action on the M^{pro} protease (Macchiagodena et al., 2022; Ahmad et al., 2021; Pavan et al., 2021; Vandyck and Deval, 2021; Zhao et al., 2021). However, in this study we have found through the use of blind docking that PF-07321332 can bind more strongly through non-covalent interactions in another distant region in the monomer mMpro, which in turn is the same site where the ivermectin B1a homologue also binds. An interesting result is that all the theoretical methods used suggest that this bonding is thermodynamically more feasible at that site in a non-covalent way than the covalent complex in the catalytic region (see supplementary material - Table S1). There is no report that has considered the effect of this on volumetric properties and its possible effect on dimerization of monomer. We have found from a thermodynamic point of view through these volumetric results that this non-covalent complex of the PF-07321332 with the monomer can significantly affect the dimerization reaction, but its comparison with

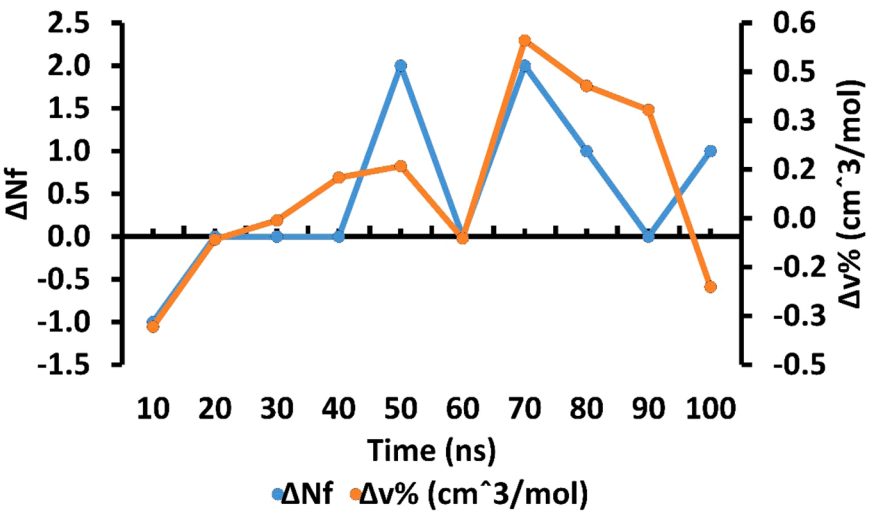

Fig. 10. Comparison between the difference $\Delta N_f = N_f^{nc} - N_f^c$ in the number of flexible fragments of non-covalent complex N_f^{nc} and covalent complex N_f^c of PF-07321332 with mM^{pro} in the same site of B1a homologue of ivermectin and in the catalytic site of mM^{pro}, respectively, and the difference between the Voronoi volume change percentage ($\Delta V\% = \left(\frac{V_p^{nh}(nc) - V_p^{nh}(c)}{V_p^{nh}(nc)}\right)100$) of the PF-07321332 (covalent bonding) and PF-07321332 (non-covalent bonding) complexes with the mM^{pro}. The predictions correspond to the minimum energy structures at 100 ns MD simulation.

the covalent complex is not possible due to lack of data.

To overcome this difficulty, we performed a comparative volumetric study between the Voronoi volume of non-covalent complex $V_p^{nh}(nc)$ at the B1 homologue site of ivermectin and the covalently bound complex $V_p^{nh}(c)$ at the catalytic site in the monomer. Interestingly, it was found that the Voronoi volumes between both species is very similar throughout the dynamic regime evaluated up to 100 ns. For clarity in Fig. 10 the percentage of difference in volume of voronoi $\Delta V\% = 100\left(\frac{V_p^{nh}(nc) - V_p^{nh}(c)}{V_p^{nh}(nc)}\right)$ in $cm^3/$ mol is presented suggesting a difference between - 0.3%and + 0.5%. This result suggests that both species have the same volumetric behavior and that they should therefore induce a similar effect on the monomer too.

The dynamic behavior of the number of flexible fragments N_f between the non-covalent complex N_f^{nc} and covalent complex N_f^c was also analyzed and we estimated their difference ΔN_f at each time (t). Despite the difference in the mode of attachment and the binding site in the monomer, the structural flexibility of the monomer in each complex is similarly small (Fig. 10). In fact, with the exception of the values ΔN_f at 50 and 70 ns, the values of ΔN_f are between -1, 0 and $+1$.

The PF-07321332 binding region different from those evaluated here is described (see **Supplementary material -** Table S1). It is important to highlight that the interactions of the PF-07321332 in the site covalently linked with the aminoacid residues coincide very well with that previously reported (Macchiagodena et al., 2022; Ahmad et al., 2021; Pavan et al., 2021; Vandyck and Deval, 2021; Zhao et al., 2021).

Despite the predictions made in this study about a potential theoretical effect at the volumetric level of ivermectin similar to that of PF-07321332 on M^{pro}, it is important to point out that the usefulness of ivermectin in the treatment of COVID-19 is a subject of controversy (Reardon, 2021). Additionally, data from the I-Tech randomized clinical trial do not support the use of ivermectin for COVID-19 (Lim et al., 2022). While there are studies showing binding of ivermectin to M^{pro}, most of them are *in silico* coupling-based or *in vitro* fluorescence-based assays that are prone to false-positive results (especially given the size of this drug molecule). A recent study also suggested that this drug does not show any significant activity in human airway-derived cell models (Dinesh Kumar et al., 2021).

On the other hand, the controversy increases because ivermectin has been included in clinical trials that have shown promising results (Carvallo and Hirsch, 2020) (https://clinicaltrials.gov/ct2/show/NCT04425863 - ClinicalTrials.gov Identifier: NCT04425863) and in collective reviews of multiple efforts that have suggested that ivermectin may have a prophylactic effect and would be a strong candidate for clinical trials to treat SARS-CoV-2 (Low et al., 2022), as also observed in systematic reviews and meta-analyses of randomized clinical trial studies (Hariyanto et al., 2022). In addition, general descriptions of the possible mechanisms of action have been provided based on experimental and computational studies that have suggested a multi-target mechanism of ivermectin against SARS-CoV-2 (Patil et al., 2022; Jeffreys et al., 2022). Physiological models have even been recently developed to reproduce SARS-CoV-2 infection using cell suspensions directly from primary human lung tissues (HLT) and have shown both promising (Grau-Expósito et al., 2022) and contradictory (Peralta-Garcia et al., 2021) results for ivermectin. This type of inconsistency in *in vitro* assays has even led to the study of various cell types from experimental data to offer physiological models with a reproducible propensity for infection, depending on the expression levels and type of receptors associated with infection SARS-CoV − 2, especially when seeking to evaluate the antiviral activity of drugs (González-Paz et al., 2022). Our team is currently working in this direction.

In this sense, multiple authors have suggested continuing studies of ivermectin and its interactions with the various targets of SARS-CoV-2 in order to use it as a model to guide efforts towards the development of new compounds and treatment strategies (Patil et al., 2022; Jeffreys et al., 2022; Delandre et al., 2022) as has already been done (Rabie, 2021). In fact, ivermectin is currently being investigated in the UK as part of the Platform Randomized Trial of Treatments in the Community for Epidemic and Pandemic Illnesses (PRINCIPLE), the world's largest clinical trial of possible COVID-19 treatments for recovery at home and in other non-hospital settings. This trial is supported by UKRI/DHSC (UK Research and Innovation (UKRI)- Department of Health and Social Care (DHSC)) (https://www.principletrial.org/).

It is important to point out that our study did not consider the competition between ligands, so it is recommended to carry out a competitive binding study taking into account the inhibition kinetics of each compound and evaluating the effect of the association and dissociation mechanisms of each ligand on the sites of interest. However, this study focused on examining the complexes formed by the drugs once they were bound independently against the same target protein, with the aim of once the complexes were formed, to be able to evaluate by molecular dynamics the strength of the union predicted by the dockings and also take minimum energy structures every 10 ns and at 100 ns to perform an analysis of the changes induced in the volumetric and hydrodynamic properties of the M^{pro} using different validated theoretical models such as HullRad (Fleming and Fleming, 2018) and 3vee.mol (Voss and Gerstein, 2010).

Specifically, in the case of PF-07321332, the complex was

reproduced as reported in the literature in which it is reported that its complex with M^{pro} is mediated by a covalent bond and therefore its binding is covalent at the site (Zhao et al., 2021), at the same time non-covalent bonds were also predicted. While in the case of ivermectin, which is a mixture of two homologues (80:20 mixtures avermectin B1a and avermectin B1b, which differ in the presence of a secbutyl and an isopropyl group, at the C25 position, respectively), what is known in the literature, including what was reported by our work, is that its binding establishes only non-covalent bonds in the M^{pro} (González-Paz et al., 2021; Fleming and Fleming, 2018; González-Paz et al., 2021).

In this sense, we focus on further studying whether PF-07321332 and ivermectin homologues, once bound to the target protein using the same conditions and degrees of freedom in terms of blind docking, can induce volumetric and hydrodynamic changes on the M^{pro} monomer, in order to predict the possible impact on homodimerization due to the binding effect of each of these ligands in their respective binding sites. This is important because multiple theoretical studies have already been reported that predict the non-covalent interaction of various compounds in regions other than the active site of M^{pro} (Khoury et al., 2022; Unoh et al., 2022; Sulimov et al., 2020; Osipiuk et al., 2021; Lockbaum et al., 2021).

In terms of docking, the docking reported for PF-07321332 could be reproduced, and a differential docking for ivermectin homologs on M^{pro} was predicted. It was found that compound B1a and PF-07321332, although they bind differently at the same site, both induce changes in volumetric properties in a similar but not identical way. While the complex formed by the monomer and compound B1b, bound to a different site, led to volumetric and hydrodynamic changes different from those of B1a and PF-07321332. These observations are important because in the literature it is known that the volumetric and hydrodynamic study can provide information on possible mechanisms of action of various compounds (Uversky, 2020).

In this way, driven by the controversy that exists around ivermectin, it was sought to know if when comparing the volumetric and hydrodynamic changes induced by its counterparts, the resulting predictions had any difference or similarity with respect to the changes predicted for the complex formed by PF-07321332, which is an authorized and validated drug for the treatment of COVID-19 and is known to bind covalently and affect homodimerization (Zhao et al., 2021; Antonopoulou et al., 2022). Additionally, this work provides the first report of the effect of PF-07321332 on M^{pro} at a volumetric and hydrodynamic level.

The importance of our predictions is based on the fact that when an accurate thermodynamic analysis of the volumetric fluctuation is attempted to find its relationship with the compressibility of a protein, the greatest number of possible structures over time is usually used without discriminating between the different energetic conformations. However, we decided to consider for the volumetric fluctuation only the structure of minimum energy to each group of energetic conformations generated every 10 ns, to focus on a study with a qualitative comparative approach between the ligand-protein complexes.

In this sense, one of the contributions of this study is found in the section corresponding to the study of volumetric fluctuation, in which we have proposed a qualitative study to observe the volumetric behavior of the different complexes, comparing them with the predictions of the elastic net method. Despite having considered only 10 points in order to work only with the representative trend, we observed a clear relationship between the fluctuation of the flexible fragments from elastic networks and the volumetric fluctuation applying a statistical compensation in each of the measurements.

Therefore, for future studies of the volumetric fluctuation we recommend taking a larger number of structures, to compare the statistical compensation with that in protein systems, a study in which our group is currently working. Especially because part of the objective of this research was to use few points of minimum energy structures for hydrodynamic and volumetric studies, thanks to the fact that we were able to determine with few measurements (only those of minimum energy) and with an empirical approximation the values reported for protein structures diverse.

Although the previously described approach was not the central part of this study and despite being a qualitative and empirical analysis, the relationship observed between the volumetric fluctuation with the number of flexible fragments predicted by elastic networks, and with the trend regarding the thermal fluctuation of the surface electrical dipole moments of the protein is interesting.

On the other hand, although the focus of this work was based on analyzing the minimum energy structure based on what is suggested by standard studies for volumetric fluctuations, in which it suggests the possibility of working with simulations even below 100 ns (Patel et al., 2012; Surampudi and Ashbaugh, 2014; Tarus et al., 2012), however, structures with minimum energy at 200 ns were analyzed, and a trend similar to that previously predicted was observed with differences in hydrodynamic ($\Delta Rg \approx 0.03$), volumetric ($\Delta v \approx 3$ Å3) and dynamic mean values. ($\Delta RMSD \approx 2.732$ Å) not very significant (see **Supplementary material**).

Finally, as we focus on analyzing the monomer as has been done in other theoretical studies (Liang et al., 2020), in order to describe the perturbation that each of these ligands could induce on the main block of the main protease (the monomer) of SARS-CoV-2, and how these interactions can cause volumetric and hydrodynamic perturbation of homodimerization, especially, since M^{pro} is known to depend on homodimerization for its biological activity (Goyal and Goyal, 2020; Tekpinar and Yildirim, 2021). However, as the interest of various efforts is the inhibition of M^{pro} by blocking or perturbing the active site (Liang et al., 2020), we recommend, to perform the analyzes proposed here on the dimeric form of M^{pro}, since the catalytic pocket of a monomer is capped at the N-terminus of the adjacent unit, as has also been done (Azam et al., 2021).

5. Conclusions

The results obtained in this work show that the binding of Paxlovid (PF, PF-07321332) and the B1a homologue occur at the same site on the monomer, while the binding of the B1b homologue occurs at a different site on the mM^{pro}. The results show that from a volumetric point of view, the non-covalent binding of ivermectin B1a and Paxlovid to mM^{pro} occurs through the same mechanism, but different from the mechanism involved in the B1b homologue. In detail, the binding of the two ivermectin homologues (B1a and B1b) and PF induces changes in the volume of the M^{pro} monomer differently. The volume change ΔV_p that occurs in the formation of the mM^{pro}-avermectin and mM^{pro}-PF complexes have negative values regardless of the ligand bound. However, in the case of the mM^{pro}-B1b complex, ΔV_p is dominated in magnitude by the volumetric change in the interaction volume ΔV_{int} ($\Delta V_{int} < 0$). In contrast, in the case of the mM^{pro}-B1a and mM^{pro}-PF complex, ΔV_p is also negative but is dominated by the volumetric contribution because the volume of the internal cavities ($\Delta V_v < 0$).

The correlation between the obtained values of δ_h γ_{pw}, $\delta\mu_r$ and V_{int} suggest that the thermal fluctuation of the dipole moment at the protein surface has an important relationship with the attractive volumetric component interaction, protein hydration and with the interfacial tension. These results can be interpreted using the adhesive-cohesive model of protein compressibility proposed by Dadarlat-Post (Dadarlat and Post, 2001). These properties are related in their behavior with the tendency observed for the fluctuation of the partial volume of the protein, due to the role of water in the properties of the protein.

From a hydrodynamic point of view, non-covalent binding of the PF drug induces dehydration of mM^{pro} as occurs with ivermectin B1a, whereas ivermectin B1b induces hydration of the M^{pro} monomer. The mM^{pro}-B1b complex is more hydrated than the mM^{pro}, mM^{pro}-PF and mM^{pro}-B1a complexes, unlike the mM^{pro}-B1a complex, which is less

hydrated of all proteins.

The values obtained from the fluctuations of the square root of the intrinsic volume $\langle \delta V_i^2 \rangle^{1/2}$ enhances the following trend mM^{pro}-B1b > mM^{pro}-B1a > mM^{pro} > mM^{pro}-PF. This trend indicates that the binding of ivermectin homologues promotes conformational changes of the structure of mM^{pro} complexes compared to native mM^{pro}, whereas the mM^{pro}-PF complex is the least dynamic of all proteins. The similarity of this trend obtained by analyzing the fluctuation $\langle \delta N_f^2 \rangle^{1/2}$ of the number of flexible fragments (N_f) using the Anisotropic and Gaussian elastic networks method (ANM + GNM), corroborates the relationship between structural dynamics and flexibility of protein fragments and also shows that ivermectin and PF affect both structural dynamics and structural flexibility of mM^{pro}.

The volumetric results support our previous observations from a thermodynamic and structural perturbation point of view using various computational tools based on molecular dynamics that each homologue binds at different sites and disrupts the global conformation differently. Also, the present study supports the experimental and theoretical reports previously suggesting that PF and B1a perturb the structure of mM^{pro} in a similar mechanism to each other but by a different mechanism to B1b.

To our knowledge, there are no reports in the literature where volumetric and hydrodynamic models together with the Anisotropic and Gaussian Elastic Network Model (ANM+GNM) are used to provide more information on the perturbation induced by ivermectin and the new drug PF-07321332 on the M^{pro} monomer and the possible impact on its biological action. The data obtained suggest that ivermectin homologues, ivernmectin B1a and PF particularly (which bind at the same site in the monomer), should affect the relevant biochemical reactions involving the monomer, as volumetrically important changes occur in the spatial conformation, hydration, flexibility and structural dynamics of this biomolecule (mM^{pro}) of relevance to virus infection.

Under this same study strategy, it was found that PF-07321332 can also covalently bind to another region of the monomer (a drug multi-site for M^{pro}), but both complexes have similar structural flexibility and volumetric properties. Finally, we consider that this type of study can help to understand the mechanism by which a ligand can block the homodimerization of this important monomer to form the dimeric protease dM^{pro} and in turn help in studies of activity-structure relationships for the design of new drugs.

Funding sources

This research did not receive any specific grant from funding agencies in the public, commercial, or not-for-profit sector.

CRediT authorship contribution statement

Ysaias J. Alvarado: Conceptualization, Methodology, Investigation, Writing – review & editing. **Yosmari Olivarez:** Investigation. **Carla Lossada:** Investigation. **Eddy Vera:** Investigation. **Alejandro Vivas:** Investigation. **Maria Hurtado:** Investigation. **Joan Vera-Villalobos:** Reviewing. **JLPaz:** Writing – review & editing, Writing – original draft preparation. **Marcos Loroño:** Writing – review & editing. **F.J. Torres:** Writing – review & editing. **Laura N. Jeffeys:** Writing – review & editing, Writing – original draft preparation, Investigation. **Lenin González-Paz:** Writing – review & editing, Conceptualization, Methodology, Investigation.

Declaration of Competing Interest

The authors declare that they have no known competing financial interests or personal relationships that could have appeared to influence the work reported in this paper.

References

Adhikari, A., Park, W.W., Kwon, O.H., 2020. Hydrogen-bond dynamics and energetics of biological water. Chempluschem 85 (12), 2657–2665. https://doi.org/10.1002/cplu.202000744.

Aggarwal, L., Biswas, P., 2020. Interaction volume is a measure of the aggregation propensity of amyloid-β. J. Phys. Chem. Lett. 11 (10), 3993–4000. https://doi.org/10.1021/acs.jpclett.0c00922.

Aghdam, R., Habibi, M., Taheri, G., 2021. Using informative features in machine learning based method for COVID-19 drug repurposing. J. Chemin. 13 https://doi.org/10.1186/s13321-021-00553-9.

Agrawal, P., Singh, H., Srivastava, H., Singh, S., Kishore, G., Raghava, G., 2019. Benchmarking of different molecular docking methods for protein-peptide docking. BMC Bioinform. 19 (13), 105–124. https://doi.org/10.1186/s12859-018-2449-y.

Ahmad, B., Batool, M., Ain, Q.U., Kim, M.S., Choi, S., 2021. Exploring the binding mechanism of PF-07321332 SARS-CoV-2 protease inhibitor through molecular dynamics and binding free energy simulations. Int. J. Mol. Sci. 22, 9124–9137. https://doi.org/10.3390/ijms22179124.

Al Khoury, C., Bashir, Z., Tokajian, S., Nemer, N., Merhi, G., Nemer, G., 2022. In silico evidence of beauvericin antiviral activity against SARS-CoV-2. Comput. Biol. Med. 141, 105171 https://doi.org/10.1016/j.compbiomed.2021.105171.

Alvarado, Y.J., Ballestas-Barrientos, A., Restrepo, J., Vera-Villalobos, J., Ferrer-Amado, G., Rodríguez-Lugo, P., Ferrebuz, A., Infante, M., Cubillán, N., 2015. Volume-related properties of thiophene and furan-2-carboxaldehyde phenylhydrazone derivatives in DMSO: a discussion about non-intrinsic contribution. J. Chem. Thermodyn. 85, 210–215. https://doi.org/10.1016/j.jct.2015.01.016.

Alvarado, Y.J., Ferrebuz, A., Paz, J.L., Rodriguez-Lugo, P., Restrepo, J., Romero, F., Fernández-Acuña, J., Williams, Y., Toro-Mendoza, J., 2018. Surface behavior of BSA/water/carbohydrate systems from molecular polarizability measurements. J. Phys. Chem. B 122 (15), 4231–4238. https://doi.org/10.1021/acs.jpcb.7b11998.

Alvarado, Y.J., Rodríguez-Lugo, P., Vera-Villalobos, J., Ferrer-Amado, G., Ferrebuz, A., Restrepo, J., Romero, F., 2015. Non-intrinsic contribution to the limiting partial molar volume of globular proteins in water: a study comparative between a new refractometric strategy and densitometric classical approach. Biointerface Res. Appl. Chem. 5 (1), 916–925.

Alvarado, Y.J., Vera-Parra, E., Méndez, A., Romero, F., González-Paz, L.A., Moncayo, L. S., Restrepo, J., Rodríguez-Lugo, P., Paz, J.L., Vera-Villalobos, J., 2021. Conformational change of ovalbumin induced by Surface cavity binding of N-phthaloyl gamma-aminobutyric acid derivative: a study theoretical and experimental. Bioint. Res. Appl. Chem. 11 (2), 9566–9586. https://doi.org/10.33263/briac112.95669586.

Antonopoulou, I., Sapountzaki, E., Rova, U., Christakopoulos, P., 2022. Inhibition of the main protease of SARS-CoV-2 (Mpro) by repurposing/designing drug-like substances and utilizing nature's toolbox of bioactive compounds. Comput. Struct. Biotechnol. J. https://doi.org/10.1016/j.csbj.2022.03.009.

Awoonor-Williams, E., Abu-Saleh, A., 2021. Covalent and non-covalent binding free energy calculations for peptidomimetic inhibitors of SARS-CoV-2 main protease. Phys. Chem. Chem. Phys. 23 (11), 6746–6757. https://doi.org/10.1039/D1CP00266J.

Azam, F., Eid, E., Almutairi, A., 2021. Targeting SARS-CoV-2 main protease by teicoplanin: a mechanistic insight by docking, MM/GBSA and molecular dynamics simulation. J. Mol. Struct. 1246, 131124 https://doi.org/10.1016/j.molstruc.2021.131124.

Azam, F., Taban, I.M., Eid, E.E.M., Iqbal, M., Alam, O., Khan, S., Mahmood, D., Anwar, M.J., Khalilullah, H., Khan, M.U., 2020. An *in-silico* analysis of ivermectin interaction with potential SARS-CoV-2 targets and host nuclear importin α. J. Biomol. Struct. Dyn. 1–14. https://doi.org/10.1080/07391102.2020.1841028.

Ball, P., 2017. Water is an active matrix of life for cell and molecular biology. Proc. Natl. Acad. Sci. U.S.A. 114 (51), 13327–13335. https://doi.org/10.1073/pnas.1703781114.

Barletta, G.P., Fernández-Alberti, S., 2018. Protein fluctuations and cavity changes relationship. J. Chem. Theory Comput. 14 (2), 998–1008. https://doi.org/10.1021/acs.jctc.7b00744.

Barletta, G.P., Franchini, G., Corsico, B., Fernández-Alberti, S., 2019. Fatty acid and retinol-binding protein: unusual protein conformational and cavity changes dictated by ligand fluctuations. J. Chem. Inf. Model. 59 (8), 3545–3555. https://doi.org/10.1021/acs.jcim.9b00364.

Blake, L., Soliman, M., 2014. Identification of irreversible protein splicing inhibitors as potential anti-TB drugs: insight from hybrid non-covalent/covalent docking virtual screening and molecular dynamics simulations. Med. Chem. Res. 23 (5), 2312–2323. https://doi.org/10.1007/s00044-013-0822-y.

Brovchenko, I., Andrews, M.N., Oleinikova, A., 2010. Volumetric properties of human islet amyloid polypeptide in liquid water. Phys. Chem. Chem. Phys. 12, 4233–4238. https://doi.org/10.1039/B918706E.

Carvallo, H., Hirsch, R., 2020. Ivermectin, aspirin, dexametasone and enoxaparin as treatment for COVID 19. J. Am. Med. Assoc. 200.

Chalikian, T.V., 2016. Excluded volume contribution to cosolvent-mediated modulation of macromolecular folding and binding reactions. Biophys. Chem. 209, 1–8. https://doi.org/10.1016/j.bpc.2015.11.001.

Chalikian, T.V., 2021. Does the release of hydration water come with a Gibbs energy contribution? J. Chem. Thermodyn. 158, 106409 https://doi.org/10.1016/j.jct.2021.106409.

Chalikian, T.V., Breslauer, K.J., 1996. On volume changes accompanying conformational transitions of biopolymers. Biopolymers 39 (5), 619–626. https://doi.org/10.1002/(SICI)1097-0282(199611)39:5<619::AID-BIP1>3.0.CO;2-Z.

Chalikian, T.V., Filfil, R., 2003. How large are the volume changes accompanying protein transitions and binding? Biophys. Chem. 104, 489–499. https://doi.org/10.1016/s0301-4622(03)00037-1.
Chalikian, T.V., Macgregor Jr., R.B., 2019. On empirical decomposition of volumetric data. Biophys. Chem. 246, 8–15. https://doi.org/10.1016/j.bpc.2018.12.005.
Chalikian, T.V., Totrov, M., Abagyan, R., Breslauer, K.J., 1996. The hydration of globular proteins as derived from volume and compressibility measurements, cross correlating thermodynamic and structural data. J. Mol. Biol. 260, 588–603. https://doi.org/10.1006/jmbi.1996.0423.
Chen, P., Hub, J., 2014. Validating solution ensembles from molecular dynamics simulation by wide-angle X-ray scattering data. Biophys. J. 107 (2), 435–447. https://doi.org/10.1016/j.bpj.2014.06.006.
Chhetri, A., Chettri, S., Rai, P., Sinha, B., Brahman, D., 2021. Exploration of inhibitory action of Azo imidazole derivatives against COVID-19 main protease (M^{pro}): a computational study. J. Mol. Struct. 1224, 129178 https://doi.org/10.1016/j.molstruc.2020.129178.
Choudhury, A., Das, N.C., Patra, R., Bhattacharya, M., Ghosh, P., Patra, B.C., Mukherjee, S., 2021. Exploring the binding efficacy of ivermectin against the key proteins of SARS-CoV-2 pathogenesis: and *in silico* approach. Future Virol. 16 (4), 277–291. https://doi.org/10.2217/fvl-2020-0342.
Cooper, A., 1984. Protein fluctuations and the thermodynamic uncertainty principle. Prog. Biophys. Mol. Biol. 44 (3), 181–214. https://doi.org/10.1016/0079-6107(84)90008-7.
Dadarlat, V.M., Post, C.B., 2001. Insights into protein compressibility from molecular dynamics simulations. J. Phys. Chem. B 105, 715–724. https://doi.org/10.1021/jp0024118.
Delandre, O., Gendrot, M., Jardot, P., Le Bideau, M., Boxberger, M., Boschi, C., Pradines, B., 2022. Antiviral activity of repurposing ivermectin against a panel of 30 clinical SARS-CoV-2 strains belonging to 14 variants. Pharmaceuticals 15 (4), 445. https://doi.org/10.3390/ph15040445.
Delre, P., Caporuscio, F., Saviano, M., Mangiatordi, G., 2020. Repurposing known drugs as covalent and non-covalent inhibitors of the SARS-CoV-2 papain-like protease. Front. Chem. 8, 1032. https://doi.org/10.3389/fchem.2020.594009.
Dinesh Kumar, N., Ter Ellen, B., Bouma, E., Troost, B., van de Pol, D., van der Ende-Metselaar, H., Smit, J., 2021. Moxidectin and ivermectin inhibit SARS-CoV-2 replication in Vero E6 cells but not in human primary airway epithelium cells. Antimicrob. Agents Chemother. https://doi.org/10.1128/AAC.01543-21.
Durojaye, O., Mushiana, T., Uzoeto, H., Cosmas, S., Udowo, V., Osotuyi, A., Gonlepa, M., 2020. Potential therapeutic target identification in the novel 2019 coronavirus: insight from homology modeling and blind docking study. Egypt. J. Med. Hum. Genet. 21 (1), 1–17. https://doi.org/10.1186/s43042-020-00081-5.
Emekli, U., Schneidman-Duhovny, D., Wolfson, H.J., Nussinov, R., Haliloglu, T., 2008. Hinge Prot: automated prediction of hinges in protein structures. Proteins Struct. Funct. Bioinf. 70 (4), 1219–1227. https://doi.org/10.1002/prot.21613.
Ferraz, W., Gomes, R., Novaes, A., Goulart Trossini, G., 2020. Ligand and structure-based virtual screening applied to the SARS-CoV-2 main protease: an in silico repurposing study. Future Med. Chem. 12 (20), 1815–1828. https://doi.org/10.4155/fmc-2020-0165.
Filfil, R., Ratavosi, A., Chalikian, T.V., 2004. Binding of bovine pancreatic trypsin inhibitor to trypsinogen: Spectroscopic and volumetric studies. Biochemistry 43, 1315–1322. https://doi.org/10.1021/bi030188.
Fleming, P.J., Fleming, K.G., 2018. HullRad: fast calculations of folded and disordered protein and nucleic acid hydrodynamic properties. Biophys. J. 114, 856–869. https://doi.org/10.1016/j.bpj.2018.01.002.
Fornés, J.A., 2008. Electrical fluctuations on the surfaces of proteins from hydrodynamic data. J. Colloid Interface Sci. 323, 255–259. https://doi.org/10.1016/j.jcis.2008.04.036.
Gautam, V., Chong, W., Chin, S., Zain, S., Rahman, N., Vao-soongnern, V., Lee, V., 2019. Loop dynamics behind the affinity of DARPins towards ERK2: Molecular dynamics simulations (MDs) and elastic network model (ENM). J. Mol. Liq. 274, 612–620. https://doi.org/10.1016/j.molliq.2018.10.157.
Gekko, K., Hasegawa, Y., 1986. Compressibility-structure relationship of globular proteins. Biochemistry 25 (21), 6563–6571. https://doi.org/10.1021/bi00369a034.
González-Paz, L., Alvarado, M., Hurtado-León, M., Lossada, C., Vera-Villalobos, J., Loroño, M., Alvarado, Y., 2022. Comparative study of SARS-CoV-2 infection in different cell types: Biophysical-computational approach to the role of potential receptors. Comput. Biol. Med., 105245 https://doi.org/10.1016/j.compbiomed.2022.105245.
González-Paz, L., Hurtado-León, M.L., Lossada, C., Fernández-Materán, F.V., Vera-Villalobos, J., Loroño, M., Paz, J.L., Jeffreys, L., Alvarado, Y.J., 2021. Comparative study of the interaction of ivermectin with proteins of interest associates with SARS-CoV-2: a computational and biophysical approach. Biophys. Chem. 278, 106677 https://doi.org/10.1016/j.bpc.2021.106677.
González-Paz, L., Hurtado-León, M.L., Lossada, C., Fernández-Materán, F.V., Vera-Villalobos, J., Loroño, M., Paz, J.L., Jeffreys, L., Alvarado, Y.J., 2021. Structural deformability induced in proteins of potential interest associated with COVID-19 by binding of homologues present in ivermectin: Comparative study based in elastic networks models. J. Mol. Liq. 340, 117284 https://doi.org/10.1016/j.molliq.2021.117284.
González-Paz, L.A., Lossada, C.A., Fernández-Materán, F.V., Paz, J.L., Vera-Villalobos, J., Alvarado, Y.J., 2020. Can non-steroidal anti-inflammatory drugs affect the interaction between receptor binding domain of SARS-COV-2 spike and the human ACE2 receptor? A computational biophysical study. Front. Phys. 8, 526. https://doi.org/10.3389/fphy.2020.587606.
González-Paz, L., Lossada, C., Moncayo, L., Romero, F., Paz, J., Vera-Villalobos, J., Alvarado, Y., 2021. A bioinformatics study of structural perturbation of 3CL-protease and the HR2-domain of SARS-CoV-2 induced by synergistic interaction with ivermectins. Biointerface Res. Appl. Chem. 11 (2), 9813–9826. https://doi.org/10.33263/BRIAC112.98139826.
Goyal, B., Goyal, D., 2020. Targeting the dimerization of the main protease of coronaviruses: A potential broad-spectrum therapeutic strategy. ACS Comb. Sci. 22 (6), 297–305. https://doi.org/10.1021/acscombsci.0c00058.
Grahl, M., Alcará, A., Perin, A., Moro, C., Pinto, É., Feltes, B., Ligabue-Braun, R., 2021. Evaluation of drug repositioning by molecular docking of pharmaceutical resources available in the Brazilian healthcare system against SARS-CoV-2. Inform. Med. Unlocked 23, 100539. https://doi.org/10.1016/j.imu.2021.100539.
Grau-Expósito, J., et al., 2022. Evaluation of SARS-CoV-2 entry, inflammation and new therapeutics in human lung tissue cells. PLoS Pathog. 18 (1), e1010171 https://doi.org/10.1371/journal.ppat.1010171.
Graziano, G., 2006. Non-intrinsic contribution to the partial molar volume of cavities in water. Chem. Phys. Lett. 429, 420–424. https://doi.org/10.1016/j.cplett.2006.08.065.
Graziano, G., 2006. Partial molar volumen of n-alcohols at infinite dilution in water calculated by means of scaled particle theory. J. Chem. Phys. 124, 134507 https://doi.org/10.1063/1.2186319.
Graziano, G., 2016. Temperature dependence of the pairwise association of hard spheres in water. J. Phys. Soc. Jpn. 85, 024801 https://doi.org/10.7566/JPSJ.85.024801.
Graziano, G., 2017. Energetics of the contact minimum configuration of two hard spheres in water. Chem. Phys. Lett. 685, 54–59. https://doi.org/10.1016/j.cplett.2017.07.030.
Graziano, G., 2013. On the magnitude of border thickness in the partial molar volume of cavities in water. Chem. Phys. Lett. 570, 46–49. https://doi.org/10.1016/j.cplett.2013.03.052.
Guedes, I.A., Costa, L.S.C., dos Santos, K.B., Karl, A.L.M., Rocha, G.K., Teixeira, I.M., Galheigo, M.M., Medeiros, V., Krempser, E., Custódio, F.L., Barbosa, H.J.C., Nicolás, M.F., Dardenne, L.E., 2021. Drug design and repurposing with DockThor-VS web server focusing on SARS-CoV-2 therapeutic targets and their non-synonym variants. Sci. Rep. 11 (1), 5543. https://doi.org/10.1038/s41598-021-84700-0.
Gupta, S., Jadaun, A., Kumar, H., Raj, U., Varadwaj, P., Rao, A., 2015. Exploration of new drug-like inhibitors for serine/threonine protein phosphatase 5 of Plasmodium falciparum: a docking and simulation study. J. Biomol. Struct. Dyn. 33 (11), 2421–2441. https://doi.org/10.1080/07391102.2015.1051114.
Hariyanto, T., Halim, D., Rosalind, J., Gunawan, C., Kurniawan, A., 2022. Ivermectin and outcomes from Covid-19 pneumonia: a systematic review and meta-analysis of randomized clinical trial studies. Rev. Med. Virol. 32 (2), e2265 https://doi.org/10.1002/rmv.2265.
Jeffreys, L., Pennington, S., Duggan, J., Caygill, C., Lopeman, R., Breen, A., Biagini, G., 2022. Remdesivir–ivermectin combination displays synergistic interaction with improved in vitro activity against SARS-CoV-2. Int. J. Antimicrob. Agents, 106542. https://doi.org/10.1016/j.ijantimicag.2022.106542.
Jiang, Y., Kirmizialtin, S., Sanchez, I.C., 2014. Dynamic void distribution in myoglobin and five mutants. Sci. Rep. 4, 4011. https://doi.org/10.1038/srep04011.
Jofily, P., Pascutti, P., Torres, P., 2021. Improving blind docking in DOCK6 through an automated preliminary fragment probing strategy. Molecules 26 (5), 1224. https://doi.org/10.3390/molecules26051224.
Kamerzell, T.J., Middaugh, C.R., 2008. The complex inter-relationships between protein flexibility and stability. J. Pharm. Sci. 97 (9), 3494–3517. https://doi.org/10.1002/jps.21269.
Kapoor, S., Winter, R., 2016. Pressure perturbation: A prime tool to study conformational substates and volume fluctuations of biomolecular assemblies. In: Terazima, M., Kataoka, M., Ueoka, R., Okamoto, Y. (Eds.), Molecular Science of Fluctuations toward Biological Functions. Springer, Tokyo, pp. 29–64. https://doi.org/10.1007/978-4-431-55840-8_2.
Kasahara, K., Terazawa, H., Itaya, H., Goto, S., Nakamura, H., Takahashi, T., Higo, J., 2020. myPresto/omegagene 2020: a molecular dynamics simulation engine for virtual-system coupled sampling. Biophys. Phys. 17, 140–146. https://doi.org/10.2142/biophysico.BSJ-2020013.
Kaur, A., Kaur, K., Banipal, P.K., Banipal, T.S., 2021. Investigations on the pH-dependent binding of sodium valproate with bovine serum albumin: a calorimetric, spectroscopic and volumetric approach. J. Chem. Thermodyn. 152, 106269 https://doi.org/10.1016/j.jct.2020.106269.
Kaur, A., Sharma, S., Banipal, P.K., Banipal, T.S., 2018. Probing the binding ability of vitamin B_1 with bovine serum albumin: calorimetric, light scattering, spectroscopic and volumetric studies. J. Chem. Thermodyn. 127, 59–70. https://doi.org/10.1016/j.jct.2018.07.009.
Kharakoz, D.P., 1992. Partial molar volumes of molecules of arbitrary shape and the effect of hydrogen bonding with water. J. Solut. Chem. 21 (6), 569–595. https://doi.org/10.1007/BF00649565.
Kharakoz, D.P., Sarvazyan, A.P., 1993. Hydrational and intrinsic compressibilities of globular proteins. Biopolymers 33, 11–26. https://doi.org/10.1002/bip.360330103.
Khoury, L., Jing, Z., Cuzzolin, A., Deplano, A., Loco, D., Sattarov, B., Sabbadin, D., 2022. Computationally driven discovery of SARS-CoV-2 M pro inhibitors: from design to experimental validation. Chem. Sci. https://doi.org/10.48550/arXiv.2110.05427.
Kneller, D., Li, H., Phillips, G., Weiss, K., Zhang, Q., Arnould, M., Kovalevsky, A., 2022. Covalent narlaprevir-and boceprevir-derived hybrid inhibitors of SARS-CoV-2 main protease: room-temperature X-ray and neutron crystallography, binding thermodynamics, and antiviral activity. rs-3 Res. Sq.. https://doi.org/10.21203/rs.3.rs-1318037/v1.
Knight, C., Hub, J., 2015. WAXSiS: a web server for the calculation of SAXS/WAXS curves based on explicit-solvent molecular dynamics. Nucleic Acids Res. 43 (W1), W225–W230. https://doi.org/10.1093/nar/gkv309.

Koulgi, S., Jani, V., Uppuladinne, M., Sonavane, U., Nath, A.K., Darbari, H., Joshi, R., 2021. Drug repurposing studies targeting SARS-CoV-2: an ensemble docking approach on drug target 3C-like protease ($3CL^{pro}$). J. Biomol. Struct. Dyn. 39, 5735–5755. https://doi.org/10.1080/07391102.2020.1792344.

Laage, D., Elsaesser, T., Hynes, J.T., 2017. Water dynamics in the hydration shells of biomolecules. Chem. Rev. 117 (16), 10694–10725. https://doi.org/10.1021/acs.chemrev.6b00765.

Lee, B., 1983. Partial molar volumen from the hard-sphere mixture model. J. Phys. Chem. 87, 112–118. https://doi.org/10.1021/j100224a026.

Lee, B., 1983. Calculations of fluctuations for globular models. Proc. Natl. Acad. Sci. U.S. A. 80, 622–626. https://doi.org/10.1073/pnas.80.2.622.

Liang, J., Karagiannis, C., Pitsillou, E., Darmawan, K., Ng, K., Hung, A., Karagiannis, T., 2020. Site mapping and small molecule blind docking reveal a possible target site on the SARS-CoV-2 main protease dimer interface. Comput. Biol. Chem. 89, 107372 https://doi.org/10.1016/j.compbiolchem.2020.107372.

Lim, S., Hor, C., Tay, K., Jelani, A., Tan, W., Ker, H., Ravi, T., 2022. Efficacy of ivermectin treatment on disease progression among adults with mild to moderate COVID-19 and comorbidities: the I-TECH randomized clinical trial. JAMA Intern. Med. https://doi.org/10.1001/jamainternmed.2022.0189.

Lindow, N., Baum, D., Bondar, A.N., Hege, H.C., 2013. Exploring cavity dynamics in biomolecular systems. BMC Bioinform. 14 https://doi.org/10.1186/1471-2105-14-S19-S5.

Lockbaum, G., Reyes, A., Lee, J., et al., 2021. Crystal structure of SARS-CoV-2 main protease in complex with the non-covalent inhibitor ML188. Viruses 13 (2), 174. https://doi.org/10.3390/v13020174.

Low, Z., Yip, A., Lal, S., 2022. Repositioning Ivermectin for Covid-19 treatment: Molecular mechanisms of action against SARS-CoV-2 replication. Biochim. Et Biophys. Acta (BBA)-Mol. Basis Dis. 1868 (2), 166294 https://doi.org/10.1016/j.bbadis.2021.166294.

Luong, T.Q., Kapoor, S., Winter, R., 2015. Pressure—a gateway to fundamental insights into protein solvation, dynamics, and function. Chemphyschem 16, 3555–3571. https://doi.org/10.1002/cphc.201500669.

Macchiagodena, M., Pagliai, M., Procacci, P., 2022. Characterization of the non-covalent interaction between the PF-07321332 inhibitor and the SARS-CoV-2 main protease. J. Mol. Graph. Model. 110, 108042 https://doi.org/10.1016/j.jmgm.2021.108042.

Madhavi, W., Weerasinghe, S., Momot, K., 2021. Reorientational dynamics of molecules in liquid methane: a molecular dynamics simulation study. J. Mol. Liq. 324, 114727 https://doi.org/10.1016/j.molliq.2020.114727.

Mahdian, S., Zarrabi, M., Panahi, Y., Dabbagh, S., 2021. Repurposing FDA-approved drugs to fight COVID-19 using in silico methods: targeting SARS-CoV-2 RdRp enzyme and host cell receptors (ACE2, CD147) through virtual screening and molecular dynamic simulations. Inform. Med. Unlocked 23, 100541. https://doi.org/10.1016/j.imu.2021.100541.

Marchi, M., 2003. Compressibility of cavities and biological water from Voronoi volumes in hydrated proteins. J. Phys. Chem. B 107, 6598–6602. https://doi.org/10.1021/jp0342935.

Mejía-Tamayo, V., Nigen, M., Apolinar-Valiente, R., Doco, T., Williams, P., Renard, D., Sanchez, C., 2018. Flexibility and hydration of amphiphilic hyperbranched arabinogalactan-protein from plant exudate: A volumetric perspective. Colloids Interfaces 2 (1). https://doi.org/10.3390/colloids2010011.

Monkos, K., 2013. A viscometric approach of pH effect on hydrodynamic properties of human serum albumin in the normal form. Gen. Physiol. Biophys. 32, 67–78. https://doi.org/10.4149/gpb_2013011.

Monkos, K., 2004. On the hydrodynamics and temperature dependence of the solution conformation of human serum albumin from viscometry approach. Biochim. Biophys. Acta 1700, 27–34. https://doi.org/10.1016/j.bbapap.2004.03.006.

Mori, K., Seki, Y., Yamada, Y., Matsumoto, H., Soda, K., 2006. Evaluation of intrinsic compressibility of proteins by molecular dynamics simulation. J. Chem. Phys. 125, 054903 https://doi.org/10.1063/1.2219741.

Morris, G., Huey, R., Lindstrom, W., Sanner, M., Belew, R., Goodsell, D., Olson, A., 2009. AutoDock4 and AutoDockTools4: automated docking with selective receptor flexibility. J. Comput. Chem. 30 (16), 2785–2791. https://doi.org/10.1002/jcc.21256.

Osipiuk, J., Azizi, S., Dvorkin, S., Endres, M., Jedrzejczak, R., Jones, K., Joachimiak, A., 2021. Structure of papain-like protease from SARS-CoV-2 and its complexes with non-covalent inhibitors. Nat. Commun. 12 (1), 1–9. https://doi.org/10.1038/s41467-021-21060-3.

O'Boyle, N.M., Banck, M., James, C.A., Morley, C., Vandermeersch, T., Hutchinson, G.R., 2011. Open babel: an open chemical toolbox. J. Chemin. 3 https://doi.org/10.1186/1758-2946-3-33.

Panikar, S., Shoba, G., Arun, M., Sahayarayan, J.J., Nanthini, A.U.R., Chinnathambi, A., Alharbi, S.A., Nasif, O., Kim, H.J., 2021. Essential oils as an effective alternative for the treatment of COVID-19: Molecular interaction analysis of protease (M^{pro}) with pharmacokinetics and toxicological properties. J. Infect. Publ. Health 14 (5), 601–610. https://doi.org/10.1016/j.jiph.2020.12.037.

Patel, N., Dubins, D.N., Pomès, R., Chalikian, T.V., 2012. Size dependence of cavity volume: a molecular dynamics study. Biophys. Chem. 161, 46–49. https://doi.org/10.1016/j.bpc.2011.10.001.

Patil, V., Verma, S., Masand, N., 2022. Prospective mode of action of Ivermectin: SARS-CoV-2. Eur. J. Med. Chem. Rep. 4, 100018 https://doi.org/10.1016/j.ejmcr.2021.100018.

Paul, A.B., Sapienza, P.J., Zhang, J., Zuo, X., Petit, C.M., 2017. Native state volume fluctuations in proteins as a mechanism for dynamic allostery. J. Am. Chem. Soc. 139 (10), 3599–3602. https://doi.org/10.1021/jacs.6b12058.

Pavan, M., Bolcato, G., Bassani, D., Sturlese, M., Moro, S., 2021. Supervised molecular dynamics (SuMD) insights into the mechanism of action of SARS-CoV-2 main protease inhibitor PF-07321332. J. Enzym. Inhib. Med. Chem. 36 (1), 1646–1650. https://doi.org/10.1080/14756366.2021.1954919.

Peralta-Garcia, A., Torrens-Fontanals, M., Stepniewski, T., Grau-Expósito, J., Perea, D., Ayinampudi, V., Selent, J., 2021. Entrectinib—A SARS-CoV-2 inhibitor in human lung tissue (HLT) cells. Int. J. Mol. Sci. 22 (24), 13592. https://doi.org/10.3390/ijms222413592.

Pereira, B., Jain, S., Garde, S., 2006. Quantifying the protein core flexibility through analysis of cavity formation. J. Chem. Phys. 124, 074704 https://doi.org/10.1063/1.2149848.

Persson, F., Halle, B., 2018. Compressibility of the protein-water interface. J. Chem. Phys. 148 (21), 215102 https://doi.org/10.1063/1.5026774.

Petřek, M., Košinová, P., Koča, J., Otyepka, M., 2007. MOLE: a Voronoi diagram-based explorer of molecular channels, pores, and tunnels. Structure 15 (11), 1357–1363. https://doi.org/10.1016/j.str.2007.10.007.

Pfeiffer, H., Heremans, K., Wevers, M., 2008. The influence of correlated protein-water volume fluctuations on the apparent compressibility of proteins determined by ultrasonic velocimetry. Biochim. Et Biophys. Acta 1784, 1546–1551. https://doi.org/10.1016/j.bbapap.2008.08.002.

Rabie, A., 2021. Two antioxidant 2, 5-disubstituted-1, 3, 4-oxadiazoles (CoViTris2020 and ChloViD2020): successful repurposing against COVID-19 as the first potent multitarget anti-SARS-CoV-2 drugs. N. J. Chem. 45 (2), 761–771. https://doi.org/10.1039/D0NJ03708G.

Reardon, S., 2021. Flawed ivermectin preprint highlights challenges of COVID drug studies. Nature 596 (7871), 173–174. https://doi.org/10.1038/d41586-021-02081-w.

Reid, K.M., Yu, X., Leitner, D.M., 2021. Change in vibrational entropy with change in protein volume estimated with mode Grüneisen parameters. J. Chem. Phys. 154, 055102 https://doi.org/10.1063/5.0039175.

Remsing, R.C., Xi, E., Patel, A.J., 2018. Protein hydration thermodynamics: The influence of flexibility and salt on hydrophobin II hydration. J. Phys. Chem. B 122 (13), 3635–3646. https://doi.org/10.1021/acs.jpcb.7b12060.

Richards, J.L., 1993. Viscosity and the shapes of macromolecules: a physical chemistry experiment using molecular-level models in the interpretation of macroscopic data obtained from simple measurements. J. Chem. Educ. 70 (8), 685–689. https://doi.org/10.1021/ed070p685.

Rother, K., Preissner, R., Goede, A., Frömmel, C., 2003. Inhomogeneous molecular density: Reference packing densities and distribution of cavities within proteins. Bioinformatics 19 (16), 2112–2121. https://doi.org/10.1093/bioinformatics/btg292.

Saikia, N., Jha, A., Deka, R., 2014. Molecular dynamics study on graphene-mediated pyrazinamide drug delivery onto the pncA protein. RSC Adv. 4 (47), 24944–24954. https://doi.org/10.1039/C4RA01486C.

Seyedi, S., Matyushov, D.V., 2018. Dipolar susceptibility of protein hydration shells. Chem. Phys. Lett. 713, 210–214. https://doi.org/10.1016/j.cplett.2018.10.045.

Shek, Y.L., Chalikian, T.V., 2013. Interactions of glycine betaine with proteins: insights from volume and compressibility measurements. Biochemistry 52 (4), 672–680. https://doi.org/10.1021/bi301554h.

Sirotkin, V.A., Komissarov, I.A., Khadiullina, A.V., 2012. Hydration of proteins: excess partial volumes of water and proteins. J. Phys. Chem. B 116 (13), 4098–4105. https://doi.org/10.1021/jp300726p.

Son, I., Chalikian, T.V., 2016. Volumetrically derived thermodynamic profile of interactions of urea with a native protein. Biochemistry 55 (47), 6475–6483. https://doi.org/10.1021/acs.biochem.6b00805.

Son, I., Shek, Y.L., Dubins, D.N., Chalikian, T.V., 2012. Volumetric characterization of tri-N-acetylglucosamine binding to lysozyme. Biochemistry 51 (29), 5784–5790. https://doi.org/10.1021/bi3006994.

Son, I., Shek, Y.L., Tikhomirova, A., Baltasar, E.H., Chalikian, T.V., 2014. Interactions of urea with native and unfolded proteins: a volumetric study. J. Phys. Chem. B 118 (47), 13554–13563. https://doi.org/10.1021/jp509356k.

Stank, A., Kokh, D.B., Fuller, J.C., Wade, R.C., 2016. Protein binding pocket dynamics. Acc. Chem. Res. 49 (5), 809–815. https://doi.org/10.1021/acs.accounts.5b00516.

Sulimov, A., Kutov, D., Taschilova, A., Ilin, I., Stolpovskaya, N., Shikhaliev, K., Sulimov, V., 2020. In search of non-covalent inhibitors of SARS-CoV-2 main protease: computer aided drug design using docking and quantum chemistry. Supercomput. Front. Innov. 7 (3) https://doi.org/10.14529/jsfi200305.

Surampudi, L., Ashbaugh, H., 2014. Direct evaluation of polypeptide partial molar volumes in water using molecular dynamics simulations. J. Chem. Eng. Data 59 (10), 3130–3135. https://doi.org/10.1021/je5001999.

Tang, K.E.S., Dill, K.A., 1998. Native protein fluctuations: The conformational-motion temperature and the inverse correlation of protein flexibility with protein stability. J. Biomol. Struct. Dyn. 16 (2), 397–411. https://doi.org/10.1080/07391102.1998.10508256.

Tang, Q.Y., Kaneko, K., 2020. Long-range correlation in protein dynamics: confirmation by structural data and normal mode analysis. Comput. Biol. 16 (2) https://doi.org/10.1371/journal.pcbi.1007670.

Tarus, B., Chevalier, C., Richard, C., Delmas, B., Di Primo, C., Slama-Schwok, A., 2012. Molecular dynamics studies of the nucleoprotein of influenza A virus: role of the protein flexibility in RNA binding. PLoS One 7 (1), e30038. https://doi.org/10.1371/journal.pone.0030038.

Tekpinar, M., Yildirim, A., 2021. Impact of dimerization and N3 binding on molecular dynamics of SARS-CoV and SARS-CoV-2 main proteases. J. Biomol. Struct. Dyn. 1–12. https://doi.org/10.1080/07391102.2021.1880481.

Timasheff, S.N., 2002. Protein-solvent preferential interactions, protein hydration, and the modulation of biochemical reactions by solvent components. Proc. Natl. Acad. Sci. U.S.A. 99 (15), 9721–9726. https://doi.org/10.1073/pnas.122225399.

Toleikis, Z., Sirotkin, V.A., Skvarnavičius, G., Smirnovienė, J., Roumestand, C., Matulis, D., Petrauskas, V., 2016. Volume of Hsp90 protein-ligand binding determined by fluorescent pressure shift assay, densitometry, and NMR. J. Phys. Chem. B 120, 9903–9912. https://doi.org/10.1021/acs.jpcb.6b06863.

Unoh, Y., Uehara, S., Nakahara, K., Nobori, H., Yamatsu, Y., Yamamoto, S., Tachibana, Y., 2022. Discovery of S-217622, a noncovalent oral SARS-CoV-2 3CL protease inhibitor clinical candidate for treating COVID-19. J. Med. Chem. https://doi.org/10.1021/acs.jmedchem.2c00117.

Uversky, V., 2020. Intrinsically disordered proteins: targets for the future? Struct. Biol. Drug Discov.: Methods Tech. Pract. 587–612. https://doi.org/10.1002/9781118681121.ch25.

Vandyck, K., Deval, J., 2021. Considerations for the discovery and development of 3-chymotrypsin-like cysteine protease inhibitors targeting SARS-CoV-2 infection. Curr. Opin. Virol. 49, 36–40. https://doi.org/10.1016/j.coviro.2021.04.006.

Voloshin, V.P., Medvedev, N.N., Smolin, N., Geiger, A., Winter, R., 2015. Exploring volume, compressibility and hydration changes of folded proteins upon compression. Phys. Chem. Chem. Phys. 17, 8499–8508. https://doi.org/10.1039/C5CP00251F.

Voloshin, V.P., Medvedev, N.N., Smolin, N., Geiger, A., Winter, R., 2015. Disentangling volumetric and hydrational properties of proteins. J. Phys. Chem. 119, 1881–1890. https://doi.org/10.1021/jp510891b.

Voss, N.R., Gerstein, M., 2010. 3V: Cavity, channel and cleft volume calculator and extractor. Nucleic Acids Res. 38, 555–562. https://doi.org/10.1093/nar/gkq395.

Whitten, S.T., García-Moreno E, B., Hilser, V.J., 2005. Local conformational fluctuations can modulate the coupling between proton binding and global structural transitions in proteins. Proc. Natl. Acad. Sci. U.S.A. 102 (12), 4282–4287. https://doi.org/10.1073/pnas.0407499102.

Xavier Senra, M., Fonseca, A., 2021. New tyrosinases with putative action against contaminants of emerging concern. Protein: Struct. Funct. Bioinform. 89 (9), 1180–1192. https://doi.org/10.1002/prot.26139.

Yonezawa, Y., 2013. Electrostatic properties of water models evaluated by a long-range potential based solely on the Wolf charge-neutral condition. Chem. Phys. Lett. 556, 308–314. https://doi.org/10.1016/j.cplett.2012.12.028.

Yuce, M., Cicek, E., Inan, T., Dag, A.B., Kurkcuoglu, O., Sungur, F.A., 2021. Repurposing of FDA-approved drugs against active site and potential allosteric drug-binding sites of COVID-19 main protease. Proteins Struct. Funct. Bioinform. 1–17. https://doi.org/10.1002/prot.26164.

Zhang, Z., Desdier, L.E.M., Scanlon, M.G., 2015. Ergometric studies of proteins: New insights into protein functionality in food systems. Trends Food Sci. Technol. 45 (2), 251–263. https://doi.org/10.1016/j.tifs.2015.06.006.

Zhao, Y., Fang, C., Zhang, Q., Zhang, R., Zhao, X., Duan, Y., Wang, H., Zhu, Y., Feng, L., Zhao, J., Shao, M., Yang, X., Zhang, L., Peng, C., Yang, K., Ma, D., Rao, Z., Yang, H., 2021. Crystal structure of SARS-CoV-2 main protease in complex with protease inhibitor PF-07321332. Protein Cell. https://doi.org/10.1007/s13238-021-00883-2.